

A Linear Time-Delay Scheme to Propagate Reduced Electron Density Matrices

Harish S. Bhat* Hardeep Bassi* Karnamohit Ranka† Christine M. Isborn†

March 26, 2024

Abstract

For any linear system where the unreduced dynamics are governed by unitary propagators, we derive a closed, time-delayed, linear system for a reduced-dimensional quantity of interest. We apply this method to understand the memory-dependence of reduced 1-electron density matrices in time-dependent configuration interaction (TDCI), a scheme to solve for the correlated dynamics of electrons in molecules. Though time-dependent density functional theory has established that the reduced 1-electron density possesses memory-dependence, the precise nature of this memory-dependence has not been understood. We derive a self-contained, symmetry/constraint-preserving method to propagate reduced TDCI electron density matrices. In numerical tests on two model systems (H_2 and HeH^+), we show that with sufficiently large time-delay (or memory-dependence), our method propagates reduced TDCI density matrices with high quantitative accuracy. We study the dependence of our results on time step and basis set. To derive our method, we calculate the 4-index tensor that relates reduced and full TDCI density matrices. Our calculation applies to any TDCI system, regardless of basis set, number of electrons, or choice of Slater determinants in the wave function. This calculation enables a proof that the trace of the reduced TDCI density matrix is constant and equals the number of electrons.

1 Introduction

Consider the discrete-time linear system

$$\mathbf{z}(t+1) = A(t)\mathbf{z}(t) \quad (1)$$

with initial condition $\mathbf{z}(0)$. Here $A(t) \in \mathbb{C}^{n \times n}$ and $\mathbf{z}(t) \in \mathbb{C}^n$. As we are focused on linear systems that arise in quantum mechanics, we assume that $A(t)$ is unitary for all $t \geq 0$. For fixed $R \in \mathbb{C}^{m \times n}$ with $m < n$, define the *reduced* quantity of interest

$$\mathbf{y}(t) = R\mathbf{z}(t) \in \mathbb{C}^m. \quad (2)$$

In this paper, we derive and study a closed system of equations that enables direct propagation of $\mathbf{y}(t)$. *Our goal is an improved understanding of the dynamics of $\mathbf{y}(t)$, especially its explicit dependence on past values $\mathbf{y}(s)$ for $s < t$.* Our goal differs from that of using (2) to gain computational efficiency—this goal has attracted much recent attention in the case where n is sufficiently large that direct

*Department of Applied Mathematics, University of California, Merced, CA 95343, USA

†Department of Chemistry & Biochemistry, University of California, Merced, CA 95343, USA

solution of (1) is costly, and where the reduced quantity $\mathbf{y}(t)$ contains sufficient information to enable scientific analysis/discovery.

Starting with $\mathbf{y}(t + 1)$ and using both (2) and (1), we have

$$\mathbf{y}(t + 1) = R\mathbf{z}(t + 1) = RA(t)\mathbf{z}(t). \quad (3)$$

By expressing $\mathbf{z}(t)$ in terms of $\{\mathbf{y}(t - \ell), \dots, \mathbf{y}(t - 1), \mathbf{y}(t)\}$, we will derive a closed, linear, time-delay system to propagate $\mathbf{y}(t)$. A key ingredient in this derivation will be the time-reversibility of the original dynamics (1). The idea of trading high-dimensionality of one dynamical system (1) for time-delayed dynamics in a reduced-dimensional space (3) is connected to notions from Mori-Zwanzig theory, Takens embedding theory, and Koopman operator theory. We review these connections below in Section 1.2.

1.1 Scientific Motivation

We target a specific problem in quantum chemistry, where (1) is the linear system that results from applying the time-dependent configuration interaction (TDCI) method to solve for the electron dynamics of a molecular system. In our problem, $\mathbf{z}(t)$ and $\mathbf{y}(t)$ are vectorized versions of full and reduced electron density matrices $P(t)$ and $Q(t)$, respectively. Below we will review TDCI and its relation to the time-dependent Schrödinger equation (TDSE). We show that $P(t)$ satisfies the Liouville-von Neumann equation, while $Q(t)$ does not—instead, $Q(t)$ satisfies a linear, time-delay system derived in this paper. For four different molecular systems, we study the behavior of this system as we vary parameters such as the total time delay. This enables us to quantify the explicit memory-dependence of $Q(t + 1)$ on $Q(s)$ for $s \leq t$.

Starting from the TDSE, one approach to compute reduced 1-electron densities is via time-dependent density functional theory (TDDFT) [39]. For an N -electron system, the TDSE is a partial differential equation (PDE) where the unknown is a wave function of $3N$ spatial variables (ignoring spin) and time. For the same N -electron system, TDDFT yields an evolution equation in three spatial variables plus time. Both the TDSE and TDDFT give us routes to compute 1-electron densities $\rho(\mathbf{x}, t)$. The Runge-Gross theorem establishes the existence of exchange-correlation potentials V_{xc} such that the 1-electron densities computed via TDDFT exactly match those computed from solutions of the TDSE for the same system [33]. Thus, in principle, TDDFT provides a tractable and scalable path to computing electron dynamics. In practice, because exact exchange-correlation functionals are unavailable, TDDFT practitioners use approximations that ignore memory-dependence of $V_{\text{xc}}[\rho](\mathbf{x}, t)$ on the 1-electron density $\rho(\mathbf{x}, s)$ for $s < t$ [11]. This approximation, known as the adiabatic approximation within the TDDFT community, leads to errors that have been quantified in prior work [9, 31, 13, 29, 19, 30].

Recent work has shown how to learn V_{xc} models that incorporate memory-dependence [36, 2]. These works focus on a one-dimensional model problem with two electrons. To scale these machine learning approaches to larger, three-dimensional molecular systems, it will be essential to incorporate prior knowledge regarding the memory-dependence of V_{xc} . This will enable targeted searches over neural network architectures that match physically relevant dynamics. In TDDFT, memory-dependence of V_{xc} results in time-delayed equations of motion for 1-electron Kohn-Sham orbitals. The sum of the squared magnitudes of all such 1-electron Kohn-Sham orbitals equals the reduced 1-electron density. Thus the time-delayed dynamics of reduced electron density matrices are closely aligned with the memory-dependence of V_{xc} . *Insight into the former, enabled by the methods of this paper, will improve our understanding of the latter.*

1.2 Related Work

Given a dynamical system in a high-dimensional space, Mori-Zwanzig theory produces closed systems for the time-evolution of low-dimensional observables [41, 23]. The resulting equations trade (i) non-time-delayed dynamics in the original, high-dimensional space for (ii) time-delayed dynamics in a low-dimensional space [6]. The time delays are expressed in terms of a memory kernel. Recent work has connected Mori-Zwanzig theory to Koopman operator methods, showing how to learn the memory kernel from data [20].

Our method shares with Mori-Zwanzig theory the trade-off between (i) and (ii). A key difference is that Mori-Zwanzig methods often assume that the unobserved or irrelevant variables can be treated as noise, leading to generalized Langevin equations [7, 8]. If we view the transformation from full electron density matrices $P(t)$ to reduced 1-electron density matrices $Q(t)$ as projection onto a subspace S , then the unobserved/irrelevant variables are the projection of $P(t)$ onto the orthogonal complement S^\perp . We make no assumptions regarding the dynamics of these variables; they do not appear at all in our self-contained scheme for propagating $Q(t)$. This is a key difference between our work and Mori-Zwanzig approaches. In Section 2.2, we explain this difference further through a concrete example.

Takens justified trading (i) for (ii) in the sense of establishing a sufficient criterion for how much memory is required (i.e., the number of time-delayed scalar observations) to accurately represent dynamics in the original phase space [38]. Takens' theory establishes the existence of time-delayed embeddings, but does not give methods to find them. Time-delayed embeddings are linked to Koopman operator methods, which are themselves closely connected to the dynamic mode decomposition (DMD) [18, 16, 5]. Time-delayed DMD aims to learn S that minimizes the squared error between left- and right-hand sides of

$$\mathbf{y}(t+1) = \sum_{j=0}^{\ell} S_j \mathbf{y}(t-j) = \underbrace{[S_0 \quad S_1 \quad \cdots \quad S_\ell]}_S \begin{bmatrix} \mathbf{y}(t) \\ \mathbf{y}(t-1) \\ \vdots \\ \mathbf{y}(t-\ell) \end{bmatrix} \quad (4)$$

In time-delayed DMD, one learns S from observations of $\mathbf{y}(t)$. In Section 2.1, we derive (8), structurally identical to (4) except that S is replaced by $S(t)$. The key difference between our method and time-delayed DMD is that rather than learn $S(t)$ from data, we derive $S(t)$ from first principles, leveraging the structure of (1-2).

Let $\dot{Q} = dQ/dt$ and let $[A, B] = AB - BA$ denote the commutator. In our past work, we have developed methods to learn density-dependent Hamiltonians $H(Q)$ from time series observations of reduced 1-electron density matrices $Q(t)$, under the assumption that $Q(t)$ satisfies the Liouville-von Neumann equation $i\dot{Q}(t) = [H(Q(t)), Q(t)]$ [3, 12]. The solution $Q(t)$ of the Liouville-von Neumann equation must satisfy $Q(t) = U(t)^\dagger Q(0)U(t)$, where $U(t)$ is unitary and \dagger denotes conjugate transpose; consequently, the eigenvalues of $Q(t)$ must equal those of $Q(0)$ for all $t \geq 0$.

For a particular molecular system (HeH⁺ in the STO-3G basis) with $N = 2$ electrons, we have applied TDCI methods (see Section 5.1) to compute full density matrices $P(t)$, from which we have computed reduced 1-electron matrices $Q(t)$ of size 2×2 . Let $\lambda_i(t)$ denote the i -th eigenvalue of $Q(t)$. In Figure 1, we plot the absolute deviation $|\lambda_i(t) - \lambda_i(0)|$, showing that *the eigenvalues of the $Q(t)$ matrices do not stay constant in time*. Therefore, there does not exist a Hamiltonian H such that $Q(t)$ satisfies the Liouville-von Neumann equation; the methods from our prior work [3, 12] are inapplicable. In contrast, the full density matrices $P(t)$ do satisfy the Liouville-von Neumann

equation (20). Figure 1 also shows that $\text{trace}(Q(t)) = N$, the number of electrons, a fact that we prove in Section 4.2.

A key feature of our system (1) is that $A(t)$ is unitary, leading to the reversibility of the dynamics, i.e., $\mathbf{z}(t) = A(t)^\dagger \mathbf{z}(t+1)$. The Liouville-von Neumann equation (20) that governs the dynamics of $P(t)$ is not dissipative. Hence we cannot directly apply balanced truncation methods that have been developed for open quantum systems [35, 1]. Variants of these methods, when applied to the full TDCI system, may yield substantial computational savings. This is outside the scope of the present work.

1.3 Summary of Contributions

Let us briefly summarize the contributions of the present paper. In Section 2.1, we give a general method to derive from (1-2) a self-contained linear delay equation for the propagation of $\mathbf{y}(t)$.

In Section 4, we derive several properties of reduced 1-electron density matrices that stem from TDCI. The derivations here are general with respect to the number of electrons (N), the number of atomic/molecular orbitals (K), and the number of configurations (or Slater determinants) included in the wave function (N_C). Proposition 4.1 enables concrete evaluation of the 4-index tensor that relates full CI electron density matrices to reduced 1-electron density matrices. Theorem 4.1 shows that reduced 1-electron density matrices $Q(t)$ have constant trace equal to N . Theorem 4.2 establishes a self-contained delay equation for $Q(t)$ that preserves Hermitian symmetry, constant trace, and identically zero elements. In our review of the literature, we have not seen the above results derived with the precision and generality carried out here.

We present numerical results in Section 5. First, we establish the accuracy of the $Q(t)$ matrices computed using the scheme from Theorem 4.2. For each molecular system, accuracy is controlled by the total memory length, the physical time corresponding to the maximum time delay in the evolution equation for $Q(t)$. With sufficiently large total memory length, the resulting $Q(t)$ matrices computed using our method match those computed directly from full TDCI simulations. We also quantify how the accuracy of $Q(t)$ depends on our choice of time step, basis set, and stride. A stride of k means that, in the equation to propagate $Q(t)$, we use every k -th previous reduced density matrix, up to a preset limit.

2 General Derivations

Here we present two derivations that apply to the linear system (1-2) in general form. We present these in an informal style for the sake of clarity, abstracting away the complexity of the quantum system that we present and analyze in Sections 3 and 4. The derivation in Section 2.1 clarifies the key steps of our time-delay scheme to propagate $\mathbf{y}(t)$. In Section 4.3, we revisit and refine this derivation for the quantum chemistry context. The derivation in Section 2.2 frames our problem as a partially observed linear system, enabling a comparison with Mori-Zwanzig theory.

2.1 Self-Contained Propagation of Reduced Quantities

By induction, we can use (1) to establish

$$\mathbf{z}(t - \ell) = \prod_{j=0}^{\ell-1} A(t - \ell + j)^\dagger \mathbf{z}(t). \quad (5)$$

Multiplying both sides by R and using (2) at time $t - \ell$ yields

$$\mathbf{y}(t - \ell) = R \prod_{j=0}^{\ell-1} A(t - \ell + j)^\dagger \mathbf{z}(t). \quad (6)$$

Stacking column vectors vertically and applying both (2) and (6), we obtain

$$\mathbf{Y}_\ell(t) = \begin{bmatrix} \mathbf{y}(t) \\ \mathbf{y}(t-1) \\ \mathbf{y}(t-2) \\ \vdots \\ \mathbf{y}(t-\ell) \end{bmatrix} = \begin{bmatrix} R\mathbf{z}(t) \\ R\mathbf{z}(t-1) \\ R\mathbf{z}(t-2) \\ \vdots \\ R\mathbf{z}(t-\ell) \end{bmatrix} = \underbrace{\begin{bmatrix} R \\ RA(t-1)^\dagger \\ RA(t-2)^\dagger A(t-1)^\dagger \\ \vdots \\ R \prod_{j=0}^{\ell-1} A(t - \ell + j)^\dagger \end{bmatrix}}_{M(t)} \mathbf{z}(t). \quad (7)$$

Here $M(t)$ has size $(\ell + 1)m \times n$, i.e., $\ell + 1$ block rows each of size $m \times n$. Assume that R , the first block of $M(t)$, has rank m (full rank because $m < n$). Each subsequent block of $M(t)$ has rank m , since each consists of R multiplied by a unitary matrix. Suppose that these blocks, when concatenated, yield a matrix of full rank. Then $M(t)$ will have rank n as long as $\ell \geq \lfloor n/m \rfloor - 1$. *Under this condition, the matrix $M(t)$ will have a pseudoinverse $M(t)^\dagger$ that is a one-sided left inverse.* Applying the pseudoinverse, we obtain

$$\mathbf{y}(t+1) = R\mathbf{z}(t+1) = RA(t)\mathbf{z}(t) = \underbrace{RA(t)M(t)^\dagger}_{S(t)} \mathbf{Y}_\ell(t) = S(t) \begin{bmatrix} \mathbf{y}(t) \\ \mathbf{y}(t-1) \\ \mathbf{y}(t-2) \\ \vdots \\ \mathbf{y}(t-\ell) \end{bmatrix} \quad (8)$$

This self-contained, linear, time-delay equation for the reduced variable $\mathbf{y}(t)$ underpins the present study. Note that $S(t)$ has size $m \times (\ell + 1)m$, precisely the same size as the matrix S in (4) that time-delay DMD learns. The difference between our approach and time-delay DMD is now clear: no observations of $\mathbf{y}(t)$ are needed or used to derive $S(t)$. Instead, we use (i) the unitary propagator $A(t)$, (ii) the reduction matrix R , and (iii) one SVD per time step, to compute $M(t)^\dagger$ from $M(t)$.

2.2 Connection with Partially Observed Linear Systems

To provide further mathematical motivation for the present paper, we examine the consequences of viewing (1-2) through the lens of partially observed linear systems, as in [27, Section 1]. In this subsection only, we assume $A(t) = A$ is a fixed (not time-dependent) unitary matrix. As mentioned above, we assume that the matrix R from (2) has rank m . Further suppose there exists a matrix \tilde{R} of size $(n - m) \times n$ such that the square $n \times n$ matrix $\mathbf{R} = \begin{bmatrix} R \\ \tilde{R} \end{bmatrix}$ has rank n . Then

$$\begin{bmatrix} \mathbf{y}(t) \\ \tilde{\mathbf{y}}(t) \end{bmatrix} = \mathbf{R}\mathbf{z}(t) \implies \mathbf{z}(t) = \mathbf{R}^{-1} \begin{bmatrix} \mathbf{y}(t) \\ \tilde{\mathbf{y}}(t) \end{bmatrix}.$$

With this, we have

$$\begin{bmatrix} \mathbf{y}(t+1) \\ \tilde{\mathbf{y}}(t+1) \end{bmatrix} = \mathbf{R}\mathbf{z}(t+1) = \mathbf{R}A\mathbf{z}(t) = \underbrace{\mathbf{R}A\mathbf{R}^{-1}}_B \begin{bmatrix} \mathbf{y}(t) \\ \tilde{\mathbf{y}}(t) \end{bmatrix}$$

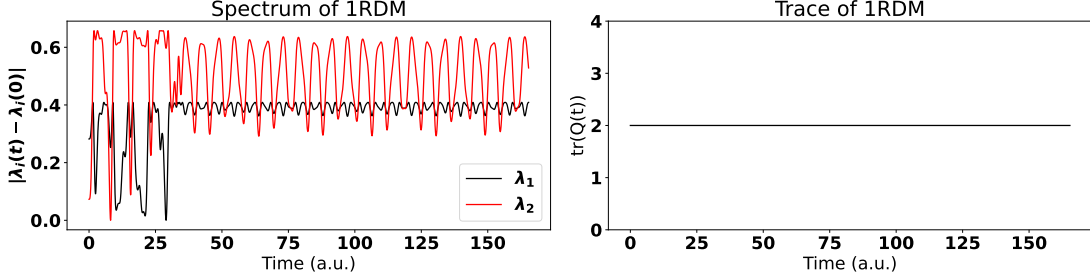


Figure 1: For the molecule HeH^+ in the STO-3G basis, we apply the methods described in Section 5.1 to compute reduced 1-electron density matrices $Q(t)$. From the left plot, we conclude that the eigenvalues of $Q(t)$ do not stay constant in time, implying that $Q(t)$ cannot satisfy the Liouville-von Neumann equation for *any* choice of Hamiltonian $H(t)$. The right plot shows that $\text{trace}(Q(t)) = 2$. Since HeH^+ has $N = 2$ electrons, this agrees with $\text{trace}(Q(t)) = N$, which we prove in Section 4.2.

Now we partition the $n \times n$ matrix B into blocks that match the sizes of \mathbf{y} and $\tilde{\mathbf{y}}$: B_{11} is $m \times m$, B_{12} is $m \times (n - m)$, B_{21} is $(n - m) \times m$, and B_{22} is $m \times m$. Then the previous equation becomes

$$\begin{bmatrix} \mathbf{y}(t+1) \\ \tilde{\mathbf{y}}(t+1) \end{bmatrix} = \begin{bmatrix} B_{11} & B_{12} \\ B_{21} & B_{22} \end{bmatrix} \begin{bmatrix} \mathbf{y}(t) \\ \tilde{\mathbf{y}}(t) \end{bmatrix}.$$

From this, one can derive the following time-delay evolution equation—see Eq. (2) in [27]:

$$\mathbf{y}(t+1) = B_{11}\mathbf{y}(t) + \sum_{s=0}^{t-1} B_{12}B_{22}^s B_{21}\mathbf{y}((t-1)-s) + B_{12}B_{22}^t \tilde{\mathbf{y}}(0). \quad (9)$$

This is essentially a Mori-Zwanzig equation: the three terms on the right-hand side can be viewed as (i) a non-time-delayed or Markovian term $B_{11}\mathbf{y}(t)$, (ii) a time-delayed or non-Markovian term that is a linear combination of $\{\mathbf{y}(0), \dots, \mathbf{y}(t-1)\}$, and (iii) a closure term that involves $\tilde{\mathbf{y}}$. To handle this closure term, [27] assumes that $B_{12}B_{22}^t \tilde{\mathbf{y}}(0) \rightarrow 0$. More generally, $\tilde{\mathbf{y}}(t)$ is often viewed as noise [6].

Here we note that as A is unitary and $B = \mathbf{R}A\mathbf{R}^{-1}$, the eigenvalues of B all have modulus 1. Hence we cannot expect that $B_{12}B_{22}^t \tilde{\mathbf{y}}(0) \rightarrow 0$ for generic unitary choices of A and \mathbf{R} . More generally, we cannot expect to use arguments based on retaining (or projecting onto) eigenvectors of B associated with the top k (in modulus) eigenvalues of B . It is likely that we will not be able to truncate the summation in the memory term.

In preliminary work, we implemented (9) for a system that corresponds to (1-2) with unitary A . Given R , it is up to us to form \tilde{R} such that \mathbf{R} is full rank. We found that when A is dense and unitary, for many choices of \tilde{R} , the resulting system (9) is numerically unstable for long-time propagation. When A is diagonal and unitary, long-time propagation succeeds. In this regime, we found that we cannot ignore the $\tilde{\mathbf{y}}(0)$ term; it does not decay as $t \rightarrow \infty$. Similarly, regarding the second term in (9), unless we sum over *all* past states $\mathbf{y}(s)$ for $s < t$, the resulting $\mathbf{y}(t)$ propagation is highly inaccurate.

The above provides additional mathematical/computational motivation to pursue our propagation scheme (8). In (8), there is no requirement to solve for \tilde{R} , the time delay is fixed, and we do not encounter any closure problems.

3 Background

We focus our attention on the dynamics of electrons in molecular systems under the Born-Oppenheimer approximation, in which nuclei are treated as fixed. This yields the problem of solving for the dynamics of N electrons in the field of N' nuclei. For this problem, the equation of motion is the time-dependent Schrödinger equation (TDSE)

$$i \frac{\partial}{\partial t} \Psi(\mathbf{r}_1, \mathbf{r}_2, \dots, \mathbf{r}_N, t) = \hat{H}(t) \Psi(\mathbf{r}_1, \mathbf{r}_2, \dots, \mathbf{r}_N, t), \quad (10)$$

for $\Psi : \mathbb{R}^{3N+1} \rightarrow \mathbb{C}$, the time-dependent N -electron wave function. The Hamiltonian $\hat{H}(t)$ is a self-adjoint operator that can be decomposed as $\hat{H}(t) = \hat{H}_e + \hat{V}_{\text{ext}}(t)$, the sum of the electronic Hamiltonian \hat{H}_e with an external potential operator $\hat{V}_{\text{ext}}(t)$ that models, for instance, an applied electric field. In atomic units, the electronic Hamiltonian is

$$\hat{H}_e = - \sum_{i=1}^N \frac{1}{2} \nabla_i^2 - \sum_{i=1}^N \sum_{A=1}^{N'} \frac{Z_A}{\|\mathbf{r}_i - \mathbf{z}_A\|} + \sum_{i=1}^N \sum_{j>i} \frac{1}{\|\mathbf{r}_i - \mathbf{r}_j\|}. \quad (11)$$

Here ∇_i^2 is the Laplacian over coordinates $\mathbf{r}_i \in \mathbb{R}^3$. The first term encodes the kinetic energy operators of all N electrons; the remaining terms are potential energy operators. The second term encodes all electron-nuclear Coulomb attractions, with nucleus A having charge Z_A and fixed position \mathbf{z}_A . The third term encodes all electron-electron Coulomb repulsions. For now, we have ignored spin coordinates of Ψ , as they do not appear in the Hamiltonian. For further details, consult [37, 22].

As the system (10-11) is a PDE in $3N + 1$ variables, it should not be surprising that exact solutions are unknown except when $N = 1$. For $N \geq 2$, solving (10-11) numerically presents serious challenges. Classical numerical methods such as finite differences and finite elements do not address the key issue, which is how to represent/store Ψ , a function of $3N + 1$ variables. Computational chemistry provides several methods to do this, at varying levels of approximation. One such method is configuration interaction, which we now describe.

3.1 Time-Dependent Configuration Interaction

We begin with a choice of *basis set*. As they are designed to approximate eigenfunctions of an atomic Hamiltonian, the functions in the basis set are often called *atomic orbitals*. Two basis sets commonly used for theoretical studies, which we refer to later in this paper, are STO-3G [37, §3.6.2] and 6-31G [14]. STO-3G is a minimal basis set that uses a linear combination of three Gaussians to describe a Slater type orbital. For hydrogen and helium, STO-3G provides one s-orbital for each atom. 6-31G is a double valence basis set that uses a larger number of Gaussian functions to better describe the nuclear cusp, and for hydrogen and helium provides s-orbitals of different size on each atom to deliver more flexibility for the electronic distribution. Let K denote the number of functions (atomic orbitals) in the basis set. As K increases, we approach a complete basis, yielding more accurate calculations at added computational cost.

Definition 3.1 (Coordinates, Spin, and Orbitals). *Let $\mathbf{x} = (\mathbf{r}, \sigma)$ where \mathbf{r} is a spatial coordinate and σ is a spin coordinate. Let $\{f_i(\mathbf{r})\}_{i=1}^K$ denote a set of atomic orbitals. Let $\alpha(\sigma)$ and $\beta(\sigma)$ denote two functions of σ that correspond to spin up and spin down, the two possible spin states of an electron. We take α and β to be orthonormal, i.e., $\langle \alpha, \alpha \rangle = \langle \beta, \beta \rangle = 1$ while $\langle \alpha, \beta \rangle = 0$. Let $\{\phi_i(\mathbf{r})\}_{i=1}^K$ be an orthonormal set of*

spatial molecular orbitals; each ϕ_i is a linear combination of the K atomic orbitals, i.e.,

$$\phi_i(\mathbf{r}) = \sum_{j=1}^K Y_{ij} f_j(\mathbf{r}). \quad (12)$$

For $j = 1, \dots, K$, define the orthonormal set of spin-orbitals $\{\chi_i(\mathbf{x})\}_{i=1}^{2K}$ via

$$\chi_{2j-1}(\mathbf{x}) = \phi_j(\mathbf{r})\alpha(\sigma), \quad \text{and} \quad \chi_{2j}(\mathbf{x}) = \phi_j(\mathbf{r})\beta(\sigma). \quad (13)$$

Using the 1-electron molecular spin-orbitals, we form *Slater determinants* [37, §2.2.3]. Their use is motivated by the Pauli exclusion principle, which requires that electronic wave functions be antisymmetric. Exchanging \mathbf{x}_i and \mathbf{x}_j on the left-hand side of (14) causes an exchange of rows i and j in the determinant, yielding a factor of -1 and the requisite antisymmetry.

Definition 3.2 (Slater Determinants). *Given a combination $\mathbf{i} = \{i_1, i_2, \dots, i_N\}$ of N distinct elements from $\{1, 2, \dots, 2K\}$, the N -electron Slater determinant corresponding to \mathbf{i} is*

$$\psi_{\mathbf{i}}^{SL}(\mathbf{x}_1, \mathbf{x}_2, \dots, \mathbf{x}_N) = \frac{1}{\sqrt{N!}} \begin{vmatrix} \chi_{i_1}(\mathbf{r}_1, \sigma_1) & \chi_{i_2}(\mathbf{r}_1, \sigma_1) & \cdots & \chi_{i_N}(\mathbf{r}_1, \sigma_1) \\ \chi_{i_1}(\mathbf{r}_2, \sigma_2) & \chi_{i_2}(\mathbf{r}_2, \sigma_2) & \cdots & \chi_{i_N}(\mathbf{r}_2, \sigma_2) \\ \vdots & \vdots & \ddots & \vdots \\ \chi_{i_1}(\mathbf{r}_N, \sigma_N) & \chi_{i_2}(\mathbf{r}_N, \sigma_N) & \cdots & \chi_{i_N}(\mathbf{r}_N, \sigma_N) \end{vmatrix}. \quad (14)$$

There are $\binom{2K}{N}$ possible N -electron Slater determinants; we use a subset of these to form CI (Configuration Interaction) basis functions. Let N_C denote the size of this subset.

Definition 3.3 (CI Basis). *For $1 \leq q \leq N_C \leq \binom{2K}{N}$, let $\mathbf{i}(q)$ enumerate the combinations in a fixed subset of distinct Slater determinants. Then the CI basis functions are*

$$\Psi_a^{\text{CI}} = \sum_{q=1}^{N_C} C_{aq} \psi_{\mathbf{i}(q)}^{SL} \quad \text{for } a = 1, \dots, N_C. \quad (15)$$

Given an atomic orbital basis set $\{f_j\}_{j=1}^K$, in order to proceed with concrete CI basis functions (15), we must solve numerically for the matrices Y and C in (12) and (15). That is, we must pin down the coefficients that express the molecular orbitals in terms of the atomic orbitals, and the coefficients that express the CI basis functions in terms of the N -electron Slater determinants. In CI approaches, one first solves the time-independent Hartree-Fock equations, a nonlinear eigenvalue problem, to determine Y . The resulting $\{\phi_i\}_{i=1}^K$ are used to construct Slater determinants (14). One then solves for C such that the CI basis $\{\Psi_a^{\text{CI}}\}_{a=1}^{N_C}$ is orthonormal and diagonalizes \hat{H}_e . In contrast, there exist other approaches, such as CASSCF (complete active space self-consistent field) [32], where one solves jointly for Y and C . Either way, the CI basis functions (15) are orthonormal and diagonalize the \hat{H}_e operator.

In TDCI and TDCASSCF [34, 26, 28], the time-dependent versions of CI and CASSCF, the wave function takes the following form:

$$\Psi(\mathbf{x}_1, \dots, \mathbf{x}_N, t) = \sum_{n=1}^{N_C} a_n(t) \Psi_n^{\text{CI}}(\mathbf{x}_1, \dots, \mathbf{x}_N). \quad (16)$$

Even with an incomplete (i.e., finite) set of atomic orbitals, if we use all possible Slater determinants in (16), and if we then solve for the coefficients $a_n(t)$ such that Ψ satisfies (10), what we

obtain is the exact solution of the TDSE within the finite atomic orbital basis set we chose. In particular, this solution will account for *electron correlation*, an effect that we must model if we are to use our results to improve models of the exchange-correlation potential V_{xc} in TDDFT. Repeating this procedure for increasing values of basis set size (K), Ψ will converge to the solution of the TDSE (10).

Substituting (16) into the TDSE (10) and expressing the Hamiltonian operator $\hat{H}(t)$ in the CI basis $\{\Psi_n^{\text{CI}}\}_{n=1}^{N_C}$ yields an ordinary differential equation for the time-evolution of the coefficients $\mathbf{a}(t) = [a_1(t), \dots, a_{N_C}(t)]$:

$$i \frac{d}{dt} \mathbf{a}(t) = (H_0 + V_{\text{ext}}(t)) \mathbf{a}(t) = H(t) \mathbf{a}(t). \quad (17)$$

Here H_0 and $V_{\text{ext}}(t)$ are the matrix expressions of the corresponding operators \hat{H}_e and $\hat{V}_{\text{ext}}(t)$ in the CI basis. For the problems we consider, the external potential term can be written $V_{\text{ext}}(t) = f(t)M_{\text{dip}}$, where $f(t)$ is a time-dependent field strength and M_{dip} is the dipole moment matrix. The dense, symmetric matrix M_{dip} encodes the separation of positive and negative charges within the molecule in the x , y , and z directions. Both H_0 and M_{dip} will depend on the particular molecular system that we are studying. Hence

$$H(t) = H_0 + V_{\text{ext}}(t) = H_0 + f(t)M_{\text{dip}}. \quad (18)$$

3.2 Full Density Matrix

The full density matrix corresponding to (16) is

$$P(t) = \mathbf{a}(t)\mathbf{a}(t)^\dagger. \quad (19)$$

Taking the time-derivative of both sides and using (17), we obtain

$$i \frac{dP}{dt} = [H(t), P(t)]. \quad (20)$$

This shows that the $N_C \times N_C$ full TDCI density matrix $P(t)$ satisfies the Liouville-von Neumann equation with the same Hamiltonian matrix $H(t)$ from (18). By (19), $P(t)$ is Hermitian for all t . As $H(t)$ does not depend on P , the Liouville-von Neumann equation is linear in the *entries* of P . For a matrix A of size $M \times M$, let $\text{vec}(A)$ denote its vectorized or flattened representation as an $M^2 \times 1$ vector. Then (20) can be written as

$$\frac{d}{dt} \text{vec}(P(t)) = -i\mathcal{H}(t) \text{vec}(P(t)), \quad (21)$$

where, using \otimes to denote Kronecker product, $\mathcal{H}(t) = I \otimes H(t) - H(t)^T \otimes I$. This is the superoperator algebra formulation of the Liouville-von Neumann equation—see [42], [24, Appendix A], and [21, §3.4.3]. Suppose we fix $\Delta t > 0$ and discretize (21) in time using the first-order scheme

$$\text{vec}(P(t + \Delta t)) = \exp(-i\mathcal{H}(t)\Delta t) \text{vec}(P(t)). \quad (22)$$

With \oplus denoting Kronecker sum, we have

$$\exp(-i\mathcal{H}(t)\Delta t) = \exp((iH(t)^T \Delta t) \oplus (-iH(t)\Delta t)) = \exp(iH(t)^T \Delta t) \otimes \exp(-iH(t)\Delta t), \quad (23)$$

a unitary matrix of size $N_C^2 \times N_C^2$. Hence we can identify $\exp(-i\mathcal{H}(t))$ with $A(t)$ in (1), and further identify $\text{vec}(P(t + \Delta t))$ and $\text{vec}(P(t))$ with $\mathbf{z}(t + 1)$ and $\mathbf{z}(t)$, respectively.

4 Methodological Results

4.1 Reduced 1-Electron Density

To define the reduced 1-electron density matrix, we must first define density operators. Let $\mathbf{X} = (\mathbf{x}_1, \dots, \mathbf{x}_N)$. For each t , the wave function Ψ defined by (16) is an element of a complex Hilbert space \mathcal{S} with inner product $\langle F, G \rangle = \int \overline{F(\mathbf{X})} G(\mathbf{X}) d\mathbf{X}$. For the purposes of the present study, precise identification of \mathcal{S} is unimportant—all we need is the inner product.

Definition 4.1 (Full Density Operator). *For $F \in \mathcal{S}$, let F^* denote the linear functional that acts on a function $G \in \mathcal{S}$ via $F^*(G) = \langle F, G \rangle$. Then the full density operator $P_t : \mathcal{S} \rightarrow \mathcal{S}$ associated with the wave function (16) is*

$$P_t = \Psi \Psi^* = \sum_{k,\ell} a_k(t) \overline{a_\ell(t)} \Psi_k^{\text{CI}} (\Psi_\ell^{\text{CI}})^*. \quad (24)$$

If we express this operator in the orthonormal CI basis $\{\Psi_n^{\text{CI}}\}_{n=1}^{N_C}$, we obtain the full density matrix (19). To go from the full to the reduced density operator, we must marginalize.

Definition 4.2 (Marginalization). *Let $(\cdot)_1$ denote integration with respect to all spins and all spatial coordinates other than \mathbf{r}_1 . For $F \in \mathcal{S}$,*

$$(F)_1(\mathbf{r}_1) = \int F(\mathbf{X}) d\sigma_1 \cdots d\sigma_N d\mathbf{r}_2 \cdots d\mathbf{r}_N. \quad (25)$$

This is equivalent to marginalizing a joint probability density. Applying this marginalization to P_t and scaling by N , the number of electrons, we obtain the reduced density operator.

Definition 4.3 (Reduced Quantities). *Let Q_t denote the reduced density operator:*

$$Q_t = N (P_t)_1 = N \sum_{k,\ell} a_k(t) \overline{a_\ell(t)} (\Psi_k^{\text{CI}} (\Psi_\ell^{\text{CI}})^*)_1. \quad (26)$$

Expressing Q_t in the orthonormal basis of molecular orbitals $\{\phi_i(\mathbf{r})\}_{i=1}^K$ and using (19), we obtain both the $K \times K$ reduced 1-electron density matrix (1RDM) $Q(t)$ and the $N_c \times N_c \times K \times K$ tensor B :

$$Q_{b,c}(t) = \langle \phi_b, Q_t \phi_c \rangle = \sum_{k,\ell=1}^{N_C} P_{k,\ell}(t) B_{k,\ell,b,c}, \quad (27)$$

$$B_{k,\ell,b,c} = N \int \overline{\phi_b(\mathbf{r})} (\Psi_k^{\text{CI}} (\Psi_\ell^{\text{CI}})^*)_1(\mathbf{r}) \phi_c(\mathbf{r}) d\mathbf{r}, \quad (28)$$

We reshape the tensor B into a matrix of size $N_C^2 \times K^2$, which we denote as \tilde{B}^T .

The definition of Q_t is equivalent to the sum of N integrals; the j -th such integral is that of P_t with respect to all spins and spatial variables *except* for \mathbf{r}_j . As electrons are indistinguishable, all of these integrals are equal to one another, explaining the factor of N in (26).

The full density operator P_t yields the joint probability density of finding each electron with a particular spin at a particular spatial location at time t . In contrast, the reduced density operator Q_t yields the probability density of finding *an* electron (with either spin) at a particular spatial location at time t . Knowledge of the 1RDM $Q(t)$ is often sufficient to compute spectroscopic quantities that can be compared against experiments.

Before proceeding, let us briefly explain why $P(t)$ must have trace equal to 1 for all t . In quantum mechanics, the wave function $\Psi(\mathbf{X}, t)$ must be normalized, i.e., for all t , $\langle \Psi, \Psi \rangle = 1$. Inserting the CI representation (16) of Ψ into this normalization condition, and using the orthonormality of the CI basis $\{\Psi_n^{\text{CI}}\}_{n=1}^{N_C}$, we obtain

$$1 = \int \sum_{k,\ell} \overline{a_k(t)\Psi_k^{\text{CI}}(\mathbf{X})} a_\ell(t)\Psi_\ell^{\text{CI}}(\mathbf{X}) d\mathbf{X} = \sum_k \overline{a_k(t)} a_k(t) = \text{trace}(P(t)). \quad (29)$$

4.2 Computing the B Tensor

To compute the B tensor, we must carry out the integral in (28). Carrying this out in full generality boils down to marginalizing an arbitrary outer product of Slater determinants.

Proposition 4.1. *For any fixed choice of distinct Slater determinants, suppose the CI basis functions are defined by (15). Then for $1 \leq k, \ell \leq N_C$, we can compute the core of B defined by (28).*

$$(\Psi_k^{\text{CI}}(\Psi_\ell^{\text{CI}})^*)_1 = \sum_{q=1}^{N_C} \sum_{q'=1}^{N_C} C_{kq} \overline{C_{\ell q'}} \left(\psi_{\mathbf{i}(q)}^{\text{SL}} (\psi_{\mathbf{i}(q')}^{\text{SL}})^* \right)_1. \quad (30)$$

To compute the right-hand side, there are two cases. When $q = q'$,

$$\left(\psi_{\mathbf{i}(q)}^{\text{SL}} (\psi_{\mathbf{i}(q)}^{\text{SL}})^* \right)_1 = \frac{1}{N} \sum_{k=1}^N \phi_{\lceil i_k(q)/2 \rceil} \phi_{\lceil i_k(q)/2 \rceil}^*. \quad (31)$$

When $q \neq q'$, there exist integers a, a' , and Z such that $a \neq a'$ and

$$\left(\psi_{\mathbf{i}(q)}^{\text{SL}} (\psi_{\mathbf{i}(q')}^{\text{SL}})^* \right)_1 = \frac{(-1)^Z}{N} \phi_{\lceil a/2 \rceil} \phi_{\lceil a'/2 \rceil}^*. \quad (32)$$

The results (31-32), together with (30), enable a complete evaluation of B .

Proof. Returning to (14-15), let us define $\gamma^{n,q} = (\gamma_1^{n,q}, \dots, \gamma_N^{n,q})$ to be the n -th permutation of the combination $\mathbf{i}(q)$. There are $N!$ such permutations. Let the parity of the n -th permutation be p_n . With this notation and (13), we can expand the Slater determinant (14) and write

$$\psi_{\mathbf{i}(q)}^{\text{SL}}(\mathbf{X}) \psi_{\mathbf{i}(q')}^{\text{SL}}(\mathbf{X})^* = \frac{1}{N!} \sum_{n=1}^{N!} \sum_{m=1}^{N!} (-1)^{p_n} (-1)^{p_m} \prod_{j=1}^N \chi_{\gamma_j^{n,q}}(\mathbf{x}_j) \chi_{\gamma_j^{m,q'}}(\mathbf{x}_j)^* \quad (33)$$

Integrating over $\mathbf{x}_2, \dots, \mathbf{x}_N$ and using the orthonormality of the spin-orbitals, we find that the integral will vanish unless $\gamma_j^{n,q} = \gamma_j^{m,q'}$ for all $j \geq 2$. Using the Kronecker δ , we have

$$\int \psi_{\mathbf{i}(q)}^{\text{SL}}(\mathbf{X}) \psi_{\mathbf{i}(q')}^{\text{SL}}(\mathbf{X})^* d\mathbf{x}_2 \cdots d\mathbf{x}_N = \frac{1}{N!} \sum_{n=1}^{N!} \sum_{m=1}^{N!} (-1)^{p_n + p_m} \chi_{\gamma_1^{n,q}}(\mathbf{x}_1) \chi_{\gamma_1^{m,q'}}(\mathbf{x}_1)^* \prod_{j=2}^N \delta_{\gamma_j^{n,q}, \gamma_j^{m,q'}}$$

Let $\epsilon_{a,b} = 1$ if a and b are either both even or both odd; let $\epsilon_{a,b} = 0$ otherwise. Then integrating over σ_1 and using (13), we obtain

$$\left(\psi_{\mathbf{i}(q)}^{\text{SL}} (\psi_{\mathbf{i}(q')}^{\text{SL}})^* \right)_1 = \frac{1}{N!} \sum_{n=1}^{N!} \sum_{m=1}^{N!} (-1)^{p_n + p_m} \phi_{\lceil \gamma_1^{n,q}/2 \rceil} \phi_{\lceil \gamma_1^{m,q'}/2 \rceil}^* \epsilon_{\gamma_1^{n,q}, \gamma_1^{m,q'}} \prod_{j=2}^N \delta_{\gamma_j^{n,q}, \gamma_j^{m,q'}} \quad (34)$$

Essentially, the combinations $\mathbf{i}(q)$ and $\mathbf{i}(q')$ can differ in at most one slot, in which case, in the slot that differs, the numbers must either both be even or both be odd. If these conditions are not satisfied, the result will be zero. We now consider the two cases in turn.

Case I: $q = q'$, so $\mathbf{i}(q) = \mathbf{i}(q')$. If two permutations of the same set of N integers agree in $N - 1$ slots, they must be identical. For each n , there is only one value of m such that $\gamma^{m,q} = \gamma^{n,q}$. So,

$$\left(\psi_{\mathbf{i}(q)}^{\text{SL}} (\psi_{\mathbf{i}(q)}^{\text{SL}})^* \right)_1 = \frac{1}{N!} \sum_{n=1}^{N!} \phi_{\lceil \gamma_1^{n,q}/2 \rceil} \phi_{\lceil \gamma_1^{n,q}/2 \rceil}^* \quad (35)$$

Holding $\gamma_1^{n,q}$ fixed at one of its N possible values, there are $(N - 1)!$ possible permutations of $\gamma_j^{n,q}$ for $j \geq 2$. Accounting for this, (35) becomes (31)

In (31), it is possible that as k goes from 1 to N , the value $\lceil i_k(q)/2 \rceil$ repeats up to twice. This is because in a single Slater determinant, it is possible for up to two spin orbitals to share the same spatial orbital.

Case II: $q \neq q'$, so $\mathbf{i}(q) \neq \mathbf{i}(q')$. Further assume that $\mathbf{i}(q)$ and $\mathbf{i}(q')$ are not reorderings of one another; this would yield Slater determinants that differ at most by a sign, and hence would not be a good choice to include in the CI expansion (15). For a nonzero integral, there must exist unique integers $a \in \mathbf{i}(q)$, $a' \in \mathbf{i}(q')$ such that $a \neq a'$ with $\epsilon_{a,a'} = 1$.

As above, there are $(N - 1)!$ permutations $\gamma^{n,q}$ such that $\gamma_1^{n,q} = a$. For each such permutation, there is only one value of m such that $\gamma_j^{m,q'} = \gamma_j^{n,q}$ for all $j \geq 2$. Let Z be the least number of flips required to permute $\mathbf{i}(q')$ so that it matches $\mathbf{i}(q)$ in all but the first slot; then $(-1)^{p_n + p_m} = (-1)^Z$ for all permutations that yield nonzero integrals. Using these facts in (34), we obtain (32).

In (32), note that $\lceil a/2 \rceil$ must differ from $\lceil a'/2 \rceil$. To see why, consider that if $\lceil a/2 \rceil = \lceil a'/2 \rceil$, then either $a = a' + 1$ or $a' = a + 1$. Both of these cases would have resulted in different spin functions of the σ_1 spin variable; by orthogonality, this yields 0. \square

Using Proposition 4.1, we have developed Python code that computes the B tensor. This code takes as input the results of a static (time-independent) CI calculation: the coefficients Y in (12) and the coefficients C and enumeration of Slater determinants $\mathbf{i}(q)$ in (15).

Theorem 4.1 (Constant Trace). *Regardless of which Slater determinants are used to form the CI basis functions, the 1RDM $Q(t)$ has constant trace equal to N , the number of electrons in the system.*

Proof. From (27), we obtain

$$\text{trace}(Q(t)) = \sum_{k,\ell=1}^{N_C} P_{k,\ell}(t) \sum_{b=1}^K B_{k,\ell,b,b}. \quad (36)$$

From (28) and (30),

$$\sum_{b=1}^K B_{k,\ell,b,b} = N \sum_{q,q'} \sum_{b=1}^K \int \overline{\phi_b(\mathbf{r})} C_{kq} \overline{C_{\ell q'}} \left(\psi_{\mathbf{i}(q)}^{\text{SL}} (\psi_{\mathbf{i}(q')}^{\text{SL}})^* \right)_1(\mathbf{r}) \phi_b(\mathbf{r}) d\mathbf{r}.$$

Examining (32), we see that this integral will vanish in Case II, whenever $q \neq q'$. Thus we need only consider $q = q'$ (Case I), upon which (31) yields

$$\begin{aligned} \sum_{b=1}^K B_{k,\ell,b,b} &= \sum_{q=1}^{N^C} \sum_{b=1}^K \int \overline{\phi_b(\mathbf{r})} C_{kq} \overline{C_{\ell q}} \sum_{m=1}^N \phi_{\lceil i_m(q)/2 \rceil}(\mathbf{r}) \phi_{\lceil i_m(q)/2 \rceil}^*(\mathbf{r}) \phi_b(\mathbf{r}) d\mathbf{r} \\ &= \sum_{q=1}^{N^C} \sum_{b=1}^K \sum_{m=1}^N \delta_{\lceil i_m(q)/2 \rceil, b} C_{kq} \overline{C_{\ell q}} = \sum_{q=1}^{N^C} N C_{kq} \overline{C_{\ell q}} \end{aligned} \quad (37)$$

To obtain the final equality, note that for each fixed m , there is precisely one b such that $\lceil i_m(q)/2 \rceil = b$. Summing over m , we obtain N .

Next, we claim that Slater determinants themselves are orthonormal: to see this, return to (33) and integrate both sides with respect to $\mathbf{X} = (\mathbf{x}_1, \dots, \mathbf{x}_N)$. We will obtain zero unless $\gamma^{n,q} \equiv \gamma^{m,q'}$, which is impossible unless $q = q'$. In that case, the integral will be 1, i.e., $\langle \psi_{\mathbf{i}(q)}^{\text{SL}}, \psi_{\mathbf{i}(q')}^{\text{SL}} \rangle = \delta_{q,q'}$. Using this, orthonormality of the CI basis functions (16) yields

$$\delta_{ab} = \langle \Psi_a^{\text{CI}}, \Psi_b^{\text{CI}} \rangle = \sum_{q,q'=1}^{N_C} \overline{C_{aq}} C_{bq'} \langle \psi_{\mathbf{i}(q)}^{\text{SL}}, \psi_{\mathbf{i}(q')}^{\text{SL}} \rangle = \sum_{q=1}^{N_C} \overline{C_{aq}} C_{bq},$$

i.e., C is unitary. Using this, (37), (36), and $\text{trace}(P(t)) \equiv 1$, we find

$$\text{trace}(Q(t)) = \sum_{k,\ell=1}^{N_C} P_{k,\ell}(t) N \delta_{k,\ell} = N. \quad (38)$$

□

4.3 Propagating 1RDMs

Proposition 4.2. *Let $k \geq 1$ be the stride. With the Hamiltonian $H(t)$ from (18) and \tilde{B}^T from the end of Definition 4.3, set*

$$\mathcal{B}_j = \tilde{B} (C_{jk}(t)^T \otimes A_{jk}(t)) \quad (39a)$$

$$C_j(t) = \exp(-iH(t - \Delta t)\Delta t) \exp(-iH(t - 2\Delta t)\Delta t) \cdots \exp(-iH(t - j\Delta t)\Delta t) \quad (39b)$$

$$A_j(t) = \exp(iH(t - j\Delta t)\Delta t) \cdots \exp(iH(t - 2\Delta t)\Delta t) \exp(iH(t - \Delta t)\Delta t) \quad (39c)$$

$$M(t) = \begin{bmatrix} \tilde{B} \\ \mathcal{B}_1 \\ \vdots \\ \mathcal{B}_\ell \end{bmatrix} \quad \text{and} \quad \mathbf{q}_\ell(t) = \begin{bmatrix} \text{vec}(Q(t)) \\ \text{vec}(Q(t - k\Delta t)) \\ \vdots \\ \text{vec}(Q(t - \ell k\Delta t)) \end{bmatrix}. \quad (39d)$$

Suppose that $P(t)$ evolves forward in time according to (22) and (23). For ℓ sufficiently large, if $M(t)$ achieves full column rank, then the 1RDM $Q(t)$ satisfies the delay equation

$$\text{vec}(Q(t+1)) = \tilde{B} (\exp(iH(t)^T \Delta t) \otimes \exp(-iH(t)\Delta t)) M(t)^+ \mathbf{q}_\ell(t). \quad (40)$$

Here $M(t)^+$ denotes the pseudoinverse of $M(t)$.

Proof. Using \tilde{B}^T , we can reformulate (27) as $\text{vec}(Q(t))^T = \text{vec}(P(t))^T \tilde{B}^T$. Transposing both sides, we get

$$\tilde{B} \text{vec}(P(t)) = \text{vec}(Q(t)). \quad (41)$$

We can identify this with (2): $\text{vec}(Q(t))$ is $\mathbf{y}(t)$, $\text{vec}(P(t))$ is $\mathbf{z}(t)$, and \tilde{B} is R . Suppose we are interested in solving for the full TDCI density $\text{vec}(P(t))$ given the right-hand side, the reduced density $\text{vec}(Q(t))$. The problem is that \tilde{B} is of dimension $K^2 \times N_C^2$ where $K < N_C$; the resulting linear system is underdetermined. As in Section 2.1, we augment (41) by relating $\text{vec}(P(t))$ to enough past 1RDMs $\text{vec}(Q(t - j\Delta t))$ to create an overdetermined system.

By (22) and (23), we have

$$\text{vec}(P(t)) = (\exp(iH(t - \Delta t)^T \Delta t) \otimes \exp(-iH(t - \Delta t)\Delta t)) \text{vec}(P(t - \Delta t)). \quad (42)$$

Inverting, iterating, and using properties of the Kronecker product, we obtain

$$(C_j(t)^T \otimes A_j(t)) \text{vec}(P(t)) = \text{vec}(P(t - j\Delta t)). \quad (43)$$

As an aside, because H is Hermitian, $A_j(t)$ is the conjugate transpose of $C_j(t)$ —see (39c) and (39b)—implying that we need only compute one of the two at each t . Multiplying (43) through by \tilde{B} , we obtain

$$\mathcal{B}_j \text{vec}(P(t)) = \text{vec}(Q(t - jk\Delta t)). \quad (44)$$

Note that (43) and (44) are particular cases of (5) and (6). The stride k allows one to use every k -th previous 1RDM, where k need not equal 1. Using what we have defined, we form the linear system

$$M(t) \text{vec}(P(t)) = \mathbf{q}_\ell(t). \quad (45)$$

This relates the full TDCI density matrix $P(t)$ to *present and past* reduced 1-electron density matrices. The block matrix $M(t)$ on the left-hand side—a special case of $M(t)$ defined by (7)—will be of dimension $(\ell+1)K^2 \times N_C^2$. By hypothesis, for ℓ sufficiently large, $M(t)$ achieves full column rank. Hence

$$\text{vec}(P(t)) = M(t)^+ \mathbf{q}_\ell(t). \quad (46)$$

To obtain (40), we return to (22), multiply both sides by \tilde{B} , and then use (46) on the right-hand side. \square

This enables propagation of reduced 1-electron densities forward in time. While this is mathematically sound, practical implementation of this method benefits from additional steps to properly account for underlying physics, as we now describe.

4.4 Incorporating Symmetries and Constraints

The crux of the method presented above is the solution of the linear system (45). Though we have mentioned that $P(t)$ is always Hermitian and satisfies $\text{trace}(P(t)) = 1$, we have not yet made use of these symmetries/constraints.

In Figure 2, the second time-dependent coefficient (labeled $a_1(t)$ in the plot) is identically zero for HeH^+ in STO-3G. By (19), this implies that the second row and second column of $P(t)$ will be identically zero. We can view this as an additional set of constraints on $P(t)$.

In Propositions 4.3, 4.4, and 4.5, we make use of, respectively, the Hermitian symmetry of $P(t)$, constant trace of $P(t)$, and identically zero elements in $P(t)$. Each allows us to reduce the dimensionality of the linear system (45) that must be solved at each time step of (40). Combining these results, we obtain the reduced-dimensional system (52), which automatically preserves symmetries/constraints.

Recall (19), which implies that $P(t)$ is Hermitian for all t . Thus for $i \neq j$, it is redundant to solve separately for P_{ij} and P_{ji} , as we do in (46). This motivates replacing $\text{vec}(P(t))$ in (46) with a representation involving only the upper-triangular (including diagonal) entries.

Definition 4.4 (Basis for Space of Hermitian Matrices). *Let \mathbb{H} be the vector space of $N_C \times N_C$ Hermitian matrices. For $j = 1$ to $j = N_C$, let the matrix S^j be purely diagonal with $S_{kk}^j = \delta_{jk}$. Now let $\tau(j) = (\tau_1(j), \tau_2(j))$ be the j -th off-diagonal, strictly upper-triangular indicial pair, i.e., the j -th element of*

$$(1, 2), \dots, (1, N_C), (2, 3), \dots, (2, N_C), \dots, (N_C - 1, N_C).$$

For $j = 1$ to $j = N_C(N_C - 1)/2$, let S^{N_C+j} be one at indices $(\tau_1(j), \tau_2(j))$ and $(\tau_2(j), \tau_1(j))$; zero otherwise; also, let $S^{N_C(N_C+1)/2+j}$ be i and $-i$ at indices $(\tau_1(j), \tau_2(j))$ and $(\tau_2(j), \tau_1(j))$, respectively; zero otherwise.

Lemma 4.1. $S = \{S^j\}_{j=1}^{N_C^2}$ is a basis for \mathbb{H} .

Proof. All S^j matrices are orthogonal in the Frobenius inner product, implying linear independence. Given any $Z \in \mathbb{H}$, there exists $\mathbf{r} \in \mathbb{R}^{N_C^2}$ such that $Z = \sum_j r_j S^j$. To find this vector, first enumerate the diagonal entries of Z , then the real parts of the strictly upper-triangular entries, and finally the imaginary parts of the strictly upper-triangular entries. \square

For example, when $N_C = 2$, we obtain the following basis of \mathbb{H} :

$$S = \{S^1, S^2, S^3, S^4\} = \left\{ \begin{bmatrix} 1 & 0 \\ 0 & 0 \end{bmatrix}, \begin{bmatrix} 0 & 0 \\ 0 & 1 \end{bmatrix}, \begin{bmatrix} 0 & 1 \\ 1 & 0 \end{bmatrix}, \begin{bmatrix} 0 & i \\ -i & 0 \end{bmatrix} \right\}.$$

Proposition 4.3. *There exists an $N_C^2 \times N_C^2$ matrix \tilde{S} such that (45) is equivalent to*

$$M(t)\tilde{S}\mathbf{x}(t) = \mathbf{q}_\ell(t). \quad (47)$$

Hence we need only solve for $\mathbf{x}(t) \in \mathbb{R}^{N_C^2}$, rather than solving (45) for $\text{vec}(P(t)) \in \mathbb{C}^{N_C^2}$.

Proof. As each S^j is an $N_C \times N_C$ matrix, the collection S is a tensor of shape $N_C^2 \times N_C \times N_C$. Reshape S into a matrix \tilde{S} such that for all $Z \in \mathbb{H}$ with $Z = \sum_j r_j S^j$,

$$\text{vec}(Z) = \tilde{S}\mathbf{r}.$$

Explicitly, $S_{k,l}^j = \tilde{S}_{(k-1)N_C+l,j}$. Using the notation $\tilde{S}_{:,j}$ to denote the j -th column of \tilde{S} , we can equivalently say that $\tilde{S}_{:,j} = \text{vec}(S^j)$. We see that \tilde{S} gives us a real representation of \mathbb{H} . Using this representation in (45), we obtain (47). Once we solve for $\mathbf{x}(t)$, we can recover the full density matrix via $\text{vec}(P(t)) = \tilde{S}\mathbf{x}(t)$. This $P(t)$ will be perfectly Hermitian. \square

Proposition 4.4 (Preserving Constant Trace). *Accounting for $\text{trace}(P(t)) = 1$, the linear system (47) can be expressed equivalently as*

$$M'(t)\mathbf{x}_{-N_C}(t) = \mathbf{q}_\ell(t) - [M(t)\tilde{S}]_{:,N_C}, \quad (48)$$

where $M'(t)$ is of size $(\ell + 1)K^2 \times (N_C^2 - 1)$ and $\mathbf{x}_{-N_C}(t) \in \mathbb{R}^{N_C^2-1}$ denotes the result of deleting the N_C -th entry from $\mathbf{x}(t)$.

Proof. By virtue of how we have defined the $\{S^j\}$ basis, the first N_C entries of $\mathbf{x}(t)$ correspond to the real, diagonal entries of $P(t)$. Thus $\text{trace}(P(t)) = 1$ implies

$$x_{N_C}(t) = 1 - \sum_{j=1}^{N_C-1} x_j(t). \quad (49)$$

Using (49) in (47), we obtain

$$\sum_{j=1}^{N_C-1} \left([M(t)\tilde{S}]_{:,j} - [M(t)\tilde{S}]_{:,N_C} \right) x_j(t) + \sum_{j=N_C+1}^{N_C^2} [M(t)\tilde{S}]_{:,j} x_j(t) = \mathbf{q}_\ell(t) - [M(t)\tilde{S}]_{:,N_C}. \quad (50)$$

To form $M'(t)$, we start with $M(t)$ and subtract its N_C -th column $[M(t)\tilde{S}]_{:,N_C}$ from each of its first $N_C - 1$ columns. From the result, delete the N_C -th column and keep the remaining columns unchanged. With this definition of $M'(t)$, (50) is (48). After solving for $\mathbf{x}_{-N_C}(t)$, we can reconstruct $\mathbf{x}(t)$ using (49); observe that $\mathbf{x}(t)$ is an affine function of $\mathbf{x}_{-N_C}(t)$. \square

Proposition 4.5 (Eliminating Zero Elements of the Full Density Matrix). *For a given molecular system, if we know a priori (e.g., based on symmetries of the molecule) that D entries of $P(t)$ will be zero, then (48) is equivalent to*

$$M''(t)\mathbf{x}_-(t) = \mathbf{q}_\ell(t) - [M(t)\tilde{S}]_{:,N_C} =: \mathbf{b}_\ell(t), \quad (51)$$

where $M''(t)$ has shape $(\ell + 1)K^2 \times (N_C^2 - 1 - D)$ and $\mathbf{x}_-(t) \in \mathbb{R}^{N_C^2 - 1 - D}$.

Proof. Start with $M'(t)$ as constructed in Proposition 4.4. For each of the D entries of $P(t)$ that are known to be zero, eliminate the corresponding column of $M'(t)$ and the corresponding entry of $\mathbf{x}_-(t)$, resulting in matrices $M''(t)$ and vectors $\mathbf{x}_-(t)$. Here the correspondence will be with respect to the ordering of our basis elements $\{S^j\}$. \square

We can now use Propositions 4.3, 4.4, and 4.5 to give an improved version of (40), the delay equation to propagate the 1RDMs $Q(t)$.

Theorem 4.2 (Constraint-Preserving Propagation of 1RDMs). *Suppose the hypotheses of Propositions 4.3, 4.4, and 4.5 are satisfied. Suppose that, for ℓ sufficiently large, $M''(t)$ as constructed in Proposition 4.5 has full column rank. Recall $\mathbf{b}_\ell(t)$ was defined by the right-hand side of (51). Then there exists an affine map $\mathcal{A} : \mathbb{R}^{N_C^2 - 1 - D} \rightarrow \mathbb{R}^{N_C^2}$ such that the 1RDM $Q(t)$ satisfies the delay equation*

$$\text{vec}(Q(t + 1)) = \tilde{B} \underbrace{(\exp(iH(t)^T \Delta t) \otimes \exp(-iH(t) \Delta t)) \tilde{S} \mathcal{A} M''(t)^+ \mathbf{b}_\ell(t)}_{\text{vec}(P(t))}. \quad (52)$$

Proof. The proof is identical to that of Theorem 4.2 except that we replace (46) with the expression labeled $\text{vec}(P(t))$ in (52). To justify this expression, first note that recovering $\mathbf{x}_-(t)$ from $\mathbf{x}_-(t)$ requires a simple linear transformation. As described at the end of the proof of Proposition 4.4, computing $\mathbf{x}(t)$ from $\mathbf{x}_-(t)$ amounts to applying an affine transformation. Composing these maps, we obtain the affine map \mathcal{A} that satisfies $\mathbf{x}(t) = \mathcal{A}\mathbf{x}_-(t)$. As $M''(t)$ has full column rank, we can compute $\mathbf{x}_-(t) = M''(t)^+ \mathbf{b}_\ell(t)$. Our real representation of \mathbb{H} yields $\text{vec}(P(t)) = \tilde{S}\mathbf{x}(t)$. In total, we obtain $\text{vec}(P(t)) = \tilde{S}\mathcal{A}M''(t)^+ \mathbf{b}_\ell(t)$. \square

By building the trace constraint into the solution process, we guarantee that each $P(t)$ on the right-hand side of (52) has trace equal to one. By properties established in Section 4.2, this implies that (52) preserves $\text{trace}(Q(t)) = N$ for all t , as in (38).

Since $M''(t)$ has $D + 1$ fewer columns than $M(t)$, it should be easier for $M''(t)$ to achieve full column rank than it is for $M(t)$. This should improve our ability to solve the linear system (51), and thereby propagate $Q(t)$ accurately.

For the above reasons, (52) should be seen as a replacement of (40); it is the method actually used in the numerical results described below.

4.5 Characterizing the Rank of $M(t)$

Let us reexamine $M(t)$ from (45). The purpose of including additional blocks $(\mathcal{B}_1, \dots, \mathcal{B}_\ell)$ in $M(t)$ is to increase the rank of the resulting matrix. Having found numerically that for sufficiently large ℓ , $M(t)$ achieves rank equal to its number of columns, we briefly examine the question of whether (and under what hypotheses) we can prove this.

As $H(t)$ is always Hermitian, $C_j(t)^T$ and $A_j(t)$ defined by (39) will always be unitary. By (39a), \mathcal{B}_j consists of \tilde{B} multiplied by a unitary matrix. Recall that \tilde{B} is of size $K^2 \times N_C^2$ with $K < N_C$. If $\text{rank}(\tilde{B}) = K^2$, then $\text{rank}(\mathcal{B}_j) = K^2$ as well.

A simple observation is that if $(C_j(t)^T \otimes A_j(t))$ happens to be the identity matrix, then $M(t)$ will consist of \tilde{B} repeated $(\ell + 1)$ times; in this scenario, $\text{rank}(M(t)) = K^2$ for any ℓ . Thus the assumption that adding blocks *increases* the rank of $M(t)$ stems from our intuition that as t increases, the system's dynamics will move $C_j(t)^T \otimes A_j(t)$ *away* from the identity.

A quantum system's dynamics are determined by its Hamiltonian $H(t)$. If we examine (18), we see three objects about which we have made no assumptions thus far: the static Hamiltonian H_0 , the external field strength $f(t)$, and the dipole moment matrix M_{dip} . We have yet to find hypotheses on H_0 , $f(t)$ and M_{dip} that guarantee that, for sufficiently large ℓ , the matrix $M(t)$ has rank equal to N_C^2 for all $t \geq 1$.

To motivate future work, we examine the $\ell = 1$ case in more detail. For a matrix Z and a set of positive integers G , let Z^G (respectively, Z^{-G}) denote the matrix formed by selecting only those columns of Z with indices in (respectively, not in) G . Then we can give a condition under which $M(t)$ has full rank.

Proposition 4.6. *Let $\ell = 1$ and consider $M(t)$ from (45). Suppose $2K^2 \leq N_C^2$ and $\text{rank}(\tilde{B}) = K^2$. Equipped with column indices $G \subset \{1, 2, \dots, N_C^2\}$, let us form the block matrix*

$$\widehat{M} = \begin{bmatrix} \tilde{B}^G & \tilde{B}^{-G} \\ \mathcal{B}_1^G & \mathcal{B}_1^{-G} \end{bmatrix}$$

If there exists G of size $|G| = K^2$ such that (i) \tilde{B}^G has rank K^2 and (ii) the Schur complement of \tilde{B}^G of \widehat{M} has rank K^2 , then $M(t)$ has rank $2K^2$.

Proof. To study the linear independence of the rows of $M(t)$, we consider

$$x\tilde{B} + y\mathcal{B}_1 = 0. \quad (53)$$

for $x, y \in \mathbb{C}^{K^2}$. Overall, (53) is an equality of row vectors in $\mathbb{C}^{N_C^2}$. Let us restrict attention to only those columns with indices in G : $x\tilde{B}^G + y\mathcal{B}_1^G = 0$. By hypothesis, the $K^2 \times K^2$ matrix \tilde{B}^G has full rank and is thus invertible. Using this, we solve for $x = -y\mathcal{B}_1^G(\tilde{B}^G)^{-1}$. Putting this back into (53), we obtain $y(\mathcal{B}_1 - \mathcal{B}_1^G(\tilde{B}^G)^{-1}\tilde{B}) = 0$. As it is clear that subsetting on the columns in G will yield the zero matrix, we instead subset on the columns *not* in G :

$$y(\mathcal{B}_1^{-G} - \mathcal{B}_1^G(\tilde{B}^G)^{-1}\tilde{B}^{-G}) = 0.$$

The $K^2 \times (N_C^2 - K^2)$ matrix multiplying y is precisely the Schur complement of \tilde{B}^G of \widehat{M} . As this Schur complement has full rank, we conclude that $y = 0$, forcing $x = 0$. \square

More generally, all we need is for $\text{rank}(M(t))$ to increase each time we increase ℓ by 1; an increase of precisely K^2 is unnecessary. If we can reorder the columns of $M(t)$ to form the block matrix \widehat{M} with the desired properties, then we can apply the Guttman rank additivity formula—see [40, Section 0.9]—to compute the rank of $M(t)$. Both the above lemma and the Guttman formula use the Schur complement.

5 Numerical Results

How much memory ℓ do we need in order to compute accurate 1RDMs for various molecular systems? To answer this question, we propagate 1RDMs using (52) and compare the results against ground truth 1RDMs. We now detail how we conduct these tests numerically.

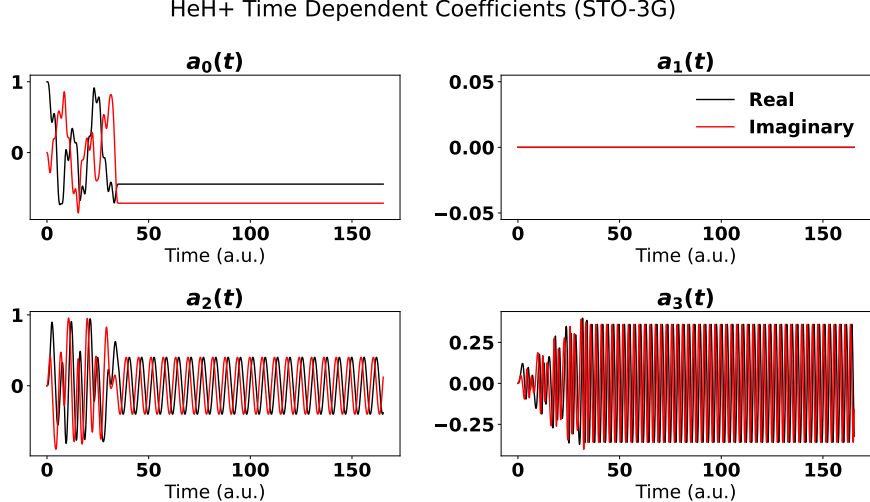


Figure 2: For the molecule HeH^+ in the STO-3G basis with $\Delta t = 0.008268$ a.u., we apply the TDCI procedure from Section 5.1 to compute the time-dependent coefficients $\mathbf{a}(t)$ for 20,000 time steps. Because $a_1(t) \equiv 0$, in the corresponding full TDCI density matrix $P(t) = \mathbf{a}(t)\mathbf{a}(t)^\dagger$, the second column and second row vanish identically. The consequences of this are explained in Section 4.4.

5.1 Procedure

Because computing full CI solutions is expensive, and as this is the first time we are studying (52), we focus attention on HeH^+ and H_2 , both with $N = 2$ electrons, in each of two basis sets: STO-3G and 6-31G. Recall that full density matrices $P(t)$ are $N_C \times N_C$ while 1RDMs $Q(t)$ are $K \times K$. For STO-3G, $N_C = 4$ and $K = 2$; for 6-31G, $N_C = 16$ and $K = 4$.

Computing ground truth 1RDMs $Q_{\text{true}}(t)$ requires some work. For a given molecular system (choice of molecule plus basis set), we apply the CASSCF method [32] with two electrons and all orbitals included in the active space to compute what is effectively a full CI solution. That is, the solution we obtain is equivalent to using all possible Slater determinants in (15). We obtain from this procedure the data needed to perform a TDCI calculation, including sets of molecular orbitals and CI basis functions, the diagonal Hamiltonian matrix H_0 and the dipole moment matrix M_{dip} —see Section 3.1 for definitions of these objects.

For each molecular system, we apply a sinusoidal external electric field. Namely, the Hamiltonian takes the form $H(t) = H_0 + f(t)M_{\text{dip}}$, for $f(t) = A \sin \omega t$. For the results reported here, for both molecules, we fix $A = 0.5$. For HeH^+ , we set $\omega = 0.9(\text{a.u.})^{-1}$ and for H_2 , we set $\omega = 1.5(\text{a.u.})^{-1}$. We apply the electric field for five cycles (approximately 35 a.u. and 21 a.u. of total time for HeH^+ and H_2 respectively), beginning at time $t = 0$. We chose these field parameters because, in our initial explorations with the STO-3G basis set, they produced electron dynamics that were the most difficult to fit.

Let $\mathbf{a}(0)$ be the unit vector such that $a_1(0) = 1$ and $a_j = 0$ for all $j \geq 2$. Then for a fixed time step $\Delta t > 0$ and a prescribed external field strength $f(t)$, we solve (17) via the scheme $\mathbf{a}(t + \Delta t) = \exp(-iH(t)\Delta t)\mathbf{a}(t)$. From this, we compute full density matrices $P_{\text{true}}(t)$ via (19). We use the methods from Sections 4.1 and 4.2 to compute the tensor B . With $P_{\text{true}}(t)$ and B , we compute $Q_{\text{true}}(t)$ via (27). The only parameters controlling the accuracy of $Q_{\text{true}}(t)$ are the choice of basis set and the time step Δt .

Computing 1RDMs with the methods developed in this paper requires setting two additional parameters: the delay length ℓ and the stride k . Recall from (39a), (44), and (45) that with delay

length ℓ and stride k , $Q(t + \Delta t)$ depends on $Q(t)$ and a total of $k\ell$ previous 1RDMs: $Q(t - jk\Delta t)$ for $j = 1, 2, \dots, \ell$. Unless stated otherwise, we set $k = 1$. Once we have set ℓ and k , we use (52) to propagate 1RDMs forward in time. As with any delay evolution equation, we must prescribe initial values on a segment. For $t < k\ell\Delta t$, we set $Q(t) = Q_{\text{true}}(t)$. We then use (52) to propagate forward in time for $t \geq k\ell\Delta t$. In what follows, we use $Q_{\text{model}}(t)$ to denote the resulting solution.

We compute $Q_{\text{true}}(t)$ and $Q_{\text{model}}(t)$ at times $t = j\Delta t$ up to $j = n_{\text{steps}}$. The final time $T = n_{\text{steps}}\Delta t$ is 165.36 a.u. This corresponds to either $n_{\text{steps}} = 2000$ with $\Delta t = 0.082680$ a.u., or $n_{\text{steps}} = 20000$ with $\Delta t = 0.008268$ a.u.

We define *memory used* or *total memory* to be the quantity $k\ell\Delta t$. This value represents the maximum time delay used by our propagation scheme, measured in atomic units (a.u.) rather than by number of time steps.

To measure the mismatch between ground truth and model 1RDMs, we use the mean-squared error (MSE) over time steps $\ell + 1, \dots, n_{\text{steps}}$. With the Frobenius norm $\|\cdot\|_F$,

$$\text{MSE} = \frac{1}{K^2} \frac{1}{n_{\text{steps}} - \ell} \sum_{j=\ell+1}^{n_{\text{steps}}} \|Q_{\text{model}}(j\Delta t) - Q_{\text{true}}(j\Delta t)\|_F^2. \quad (54)$$

We also use the mean absolute error (MAE) at each time t :

$$\text{MAE}(t) = \frac{1}{K^2} \sum_{i,j=1}^K \left| Q_{ij}^{\text{model}}(t) - Q_{ij}^{\text{true}}(t) \right|, \quad (55)$$

Scheme (52) requires solving (51) for $\mathbf{x}_-(t) = M''(t)^+ \mathbf{b}_\ell(t)$ at each time step. To measure internal error, we compute and record the *residual error* at time t :

$$\text{residual}(t) = \|M''(t)\mathbf{x}_-(t) - \mathbf{b}_\ell(t)\|_2. \quad (56)$$

5.2 Computational Resources

All computations were carried out on login and GPU nodes of the NERSC Perlmutter cluster¹. All source code required to reproduce our results is available in an online repository². Propagation scheme (52) was implemented in Python using JAX (for $k = 1$) and CuPy (for $k \geq 2$) [4, 25]. For calculations in the STO-3G basis set, the wall-clock run time of the propagation scheme ranged from 45 seconds to 20 minutes. In contrast, for calculations in the 6-31G basis set, the wall-clock run time of the propagation scheme took between 15 and 45 minutes. Run times depend primarily on the parameter ℓ ; as ℓ increases, we need more Kronecker products to propagate $Q(t)$ via (52).

5.3 Results and Discussion

Our main numerical results, summarized in Figures 3-7, quantify how propagation of 1RDMs depends on total memory $k\ell\Delta t$, time step Δt , and stride k . A key goal is to gain insight on how much total memory is required for each of our four molecular systems (HeH⁺ and H₂ in STO-3G and 6-31G) to achieve numerically acceptable levels of accuracy.

¹<https://docs.nersc.gov/systems/perlmutter/architecture/>

²https://github.com/hbassi/1rdm_memory_model

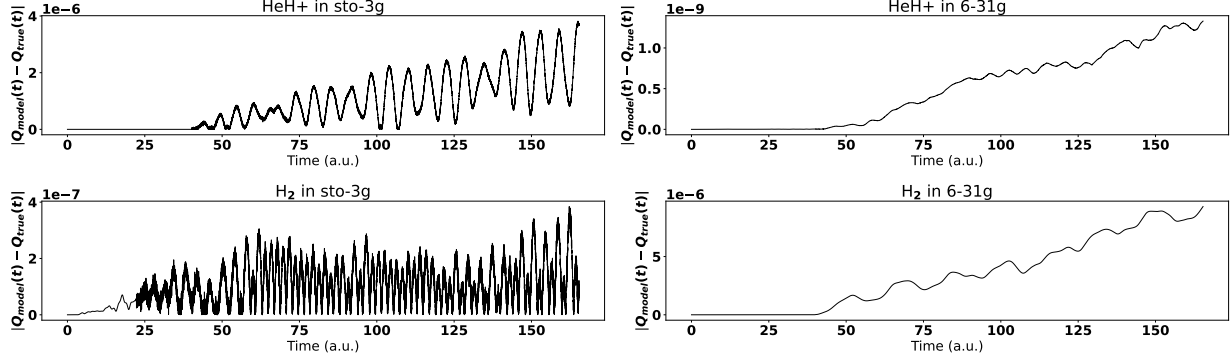


Figure 3: For each of four molecular systems we tested, with sufficiently large total memory ($k\ell\Delta t$), the 1RDMs produced by our propagation scheme (52) agree closely with ground truth 1RDMs at all times t . Each plot shows $\text{MAE}(t)$ defined by (55) versus physical time in atomic units (a.u.) From left to right, top to bottom, the maximum MAE values are bounded by 4×10^{-6} , 1.5×10^{-9} , 4×10^{-7} , and 10^{-5} ; the corresponding values for total memory are 5.3, 6.6, 0.6, and 13 a.u., respectively. For details of all other parameters, consult the text in Section 5.3.

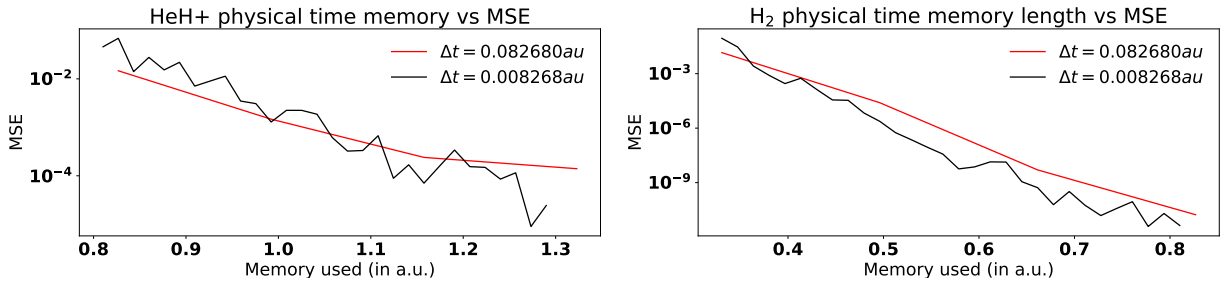


Figure 4: For each molecule in the STO-3G basis set, we fix the stride $k = 1$. For each of two choices of Δt , we plot the MSE (54) as a function of total memory $k\ell\Delta t$. Note that for both molecules, the MSE approaches zero at similar rates, regardless of Δt . This indicates that our scheme (52) identifies a physical time scale of 1RDM memory-dependence.

With sufficient memory, our time-delay propagation scheme yields highly accurate 1RDMs. Figure 3 shows that, with sufficiently large total memory ($k\ell\Delta t$), the 1RDMs produced by (52) agree closely with ground truth 1RDMs at all times t . For the results in Figure 3, $\Delta t = 0.008268$ and $n_{\text{steps}} = 20000$. Here our goal was to choose parameters such that $\text{MAE}(t)$ —as defined by (55)—drops below $O(10^{-6})$ for each molecular system. This level of accuracy demonstrates that the scheme (52) is indeed capable of computing 1RDMs that are in close quantitative agreement with ground truth 1RDMs. For HeH^+ in STO-3G and 6-31G, we used parameters of $\ell = 160$, $k = 4$ and $\ell = 160$, $k = 5$, respectively. For H_2 in STO-3G and 6-31G, we used parameters of $\ell = 72$, $k = 1$ and $\ell = 220$, $k = 7$, respectively. These values lead to total memory ($k\ell\Delta t$) of 5.3, 6.6, 0.6, and 13 a.u. for the four molecular systems considered.

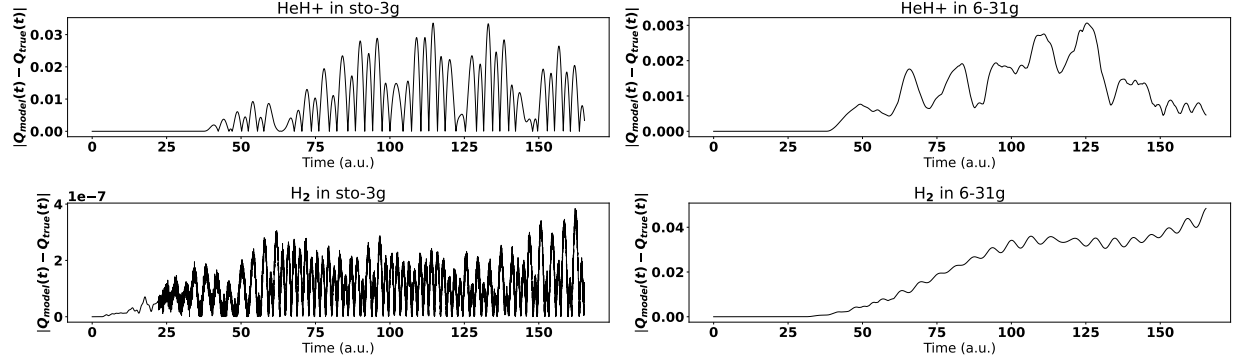
Results are approximately invariant under time step refinement. For each molecular system, we seek a physical time scale that governs memory-dependence of 1RDMs. In order to rule out that the computed time scales are numerical artifacts, we check whether our results depend on Δt . For the two molecules in STO-3G, we fix the stride to be $k = 1$ and repeatedly run simulations—using (52)—at increasing values of ℓ . We do this for both values of Δt and n_{steps} mentioned above, such that $n_{\text{steps}}\Delta t = T = 165.36$ a.u. For each choice of ℓ and Δt , we compute the MSE (54). We plot in Figure 4 the MSE versus total memory ($k\ell\Delta t$) for both choices of Δt . For both molecules, and for both choices of Δt , the MSE approaches zero as total memory increases. Moreover, the rate at which MSE approaches zero is approximately independent of Δt . This indicates that our scheme (52) identifies a physical time scale of memory-dependence for each molecular system.

With less total memory, 1RDMs retain qualitative accuracy. In Figure 5, we visualize the consequences of using less total memory for all molecular systems. We set $k = 1$, $\Delta t = 0.008268$ a.u., $n_{\text{steps}} = 20000$. For HeH^+ in STO-3G and 6-31G, we set $\ell = 160$ (total memory of 1.3 a.u.) For H_2 in STO-3G and 6-31G, we set $\ell = 72$ (total memory of 0.6 a.u.) and $\ell = 850$ (total memory of 7 a.u.), respectively. As compared with Figure 3, we use less total memory, incurring larger errors $\text{MAE}(t)$ at each time t , as shown in Figure 5a. Nonetheless, in Figure 5b, we see close agreement between the upper-left components of the 1RDM matrices $Q_{\text{true}}(t)$ (black) and $Q_{\text{model}}(t)$ (red) at each t . Other components of the 1RDM matrices feature similar agreement. We hypothesize that the qualitative match between $Q_{\text{true}}(t)$ and $Q_{\text{model}}(t)$ seen here is sufficient to calculate quantities of chemical/physical interest.

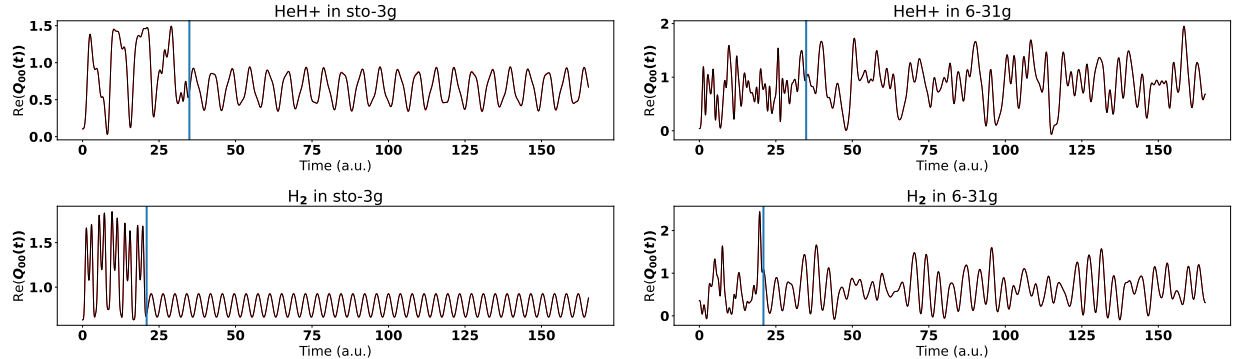
Using stride $k \geq 2$ leads to reduced propagation error. The dimensions of $M(t)$ and $\mathbf{q}_\ell(t)$ in (45) depend on ℓ but not k . Thus for fixed ℓ , increasing k enables one to increase the total memory used *without* a proportional increase in computational cost.

Above we formulated a theory that, for each molecular system, there exists a physical time scale of memory $k\ell\Delta t$. One consequence of this theory is that if we fix ℓ , fix Δt and increase k , MSE should decrease. Here we test this idea. We fix $\Delta t = 0.008268$. For HeH^+ , we set $\ell = 160$; for H_2 , we set $\ell = 220$. For each $k \in \{2, 3, 4, 5, 6, 7, 8\}$, we repeatedly run propagation scheme (52) and compute the MSE (54). Note that we omit H_2 in STO-3G as the MSE was already $O(10^{-7})$ with $k = 1$ as shown in Figures 3 and 5.

We plot the resulting MSE values against both total memory $k\ell\Delta t$ (lower horizontal axis) and stride k (upper horizontal axis) in Figure 6. We also plot, in the left and right panels, the MSE associated with the baseline value $k = 1$. In the center panel, the corresponding MSE for $k = 1$ lies well above the vertical scale of the plot. We see clear evidence that using strides $k \geq 2$ can reduce the MSE by orders of magnitude compared with $k = 1$. Given the ℓ values quoted above, each



(a) We plot MAE(t) defined by (55) for each of four molecular systems.



(b) We plot the upper-left components of the matrices $Q_{\text{true}}(t)$ (black) and $Q_{\text{model}}(t)$ (red) for each of four molecular systems.

Figure 5: For each of the four molecular systems we tested, as compared with Figure 3, we relax our desired level of accuracy. We set the stride $k = 1$ and time step $\Delta t = 0.008268$ a.u. for all systems. For HeH^+ , the total memory was 1.3 a.u. for both basis sets; for H_2 , the total memory was 0.6 and 7 a.u. in STO-3G and 6-31G, respectively. In Figure 5a, even when the MAE at each time is $O(10^{-2})$, the corresponding plots of $Q_{\text{model}}(t)$ (red) and $Q_{\text{true}}(t)$ (black) in Figure 5b are indistinguishable. In Figure 5b, the vertical blue line represents the time at which the electric field is turned off. Plots corresponding to the same molecular system were produced using the same parameter ℓ ; for these values and other details, see Section 5.3.

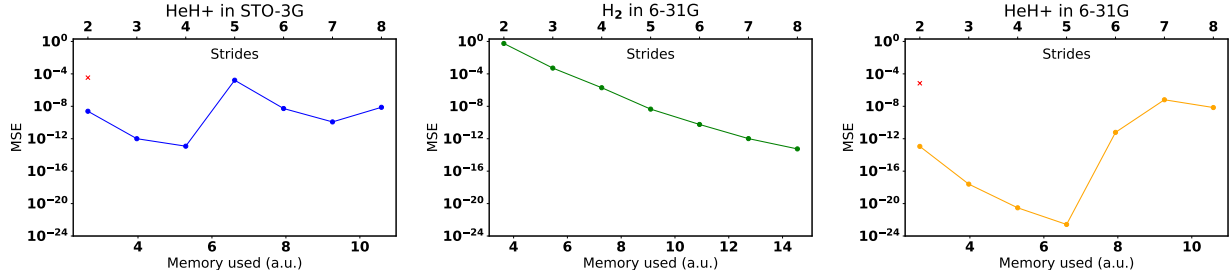


Figure 6: For the three molecular systems with higher error in Figure 5, we keep ℓ fixed and consider $k \in \{2, 3, 4, 5, 6, 7, 8\}$. For each value of k , we run our scheme (52) and compute the MSE (54). We plot the MSE both against total memory $k\ell\Delta t$ (lower horizontal axis) and stride k (upper horizontal axis). In the left and right panels, we plot the baseline $k = 1$ MSE using a single red dot. In the center panel, the baseline MSE with $k = 1$ is well above the vertical scale of the plot and hence not shown. We see that increasing stride can reduce the MSE by multiple orders of magnitude for each molecular system.

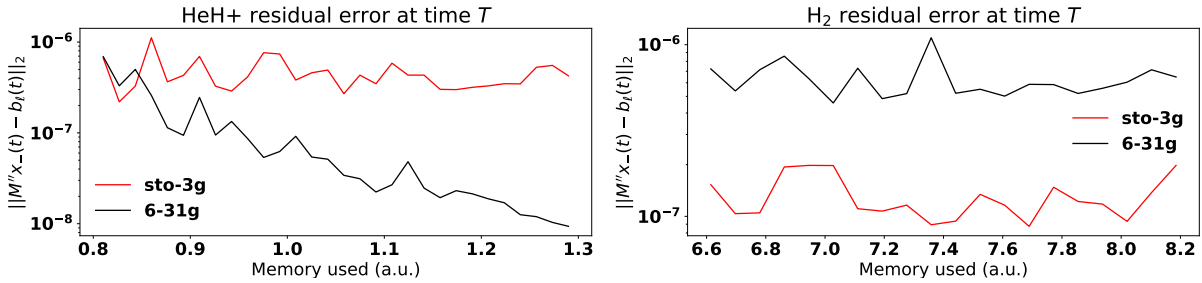


Figure 7: When we use (52) to propagate 1RDMs $Q(t)$ forward in time, we must solve the linear system (51) at each time step. For each simulation run corresponding to a different value of ℓ and fixed values of $k = 1$ and $\Delta t = 0.008268$ a.u., we compute the residual error (56) at the final time T . For each of our four molecular systems, we plot this error versus memory used ($k\ell\Delta t$). The results show that the residual errors are tolerable.

corresponding unit increase in k leads to a large increase in total memory $k\ell\Delta t$. Thus increasing k is an efficient way to boost the total memory used by the scheme (52), without incurring increased computational cost. Overall, these results support the view that scheme (52) can be made arbitrarily accurate by tuning the total memory $k\ell\Delta t$.

Residual errors for the linear system (51) are tolerable. A key assumption in our derivation of the scheme (52) was that if we add sufficiently many blocks to $M(t)$ defined by (39d), then $M''(t)$ achieves full column rank, enabling us to solve the linear system (51) accurately at each time step. To test this assumption, we again fixed $\Delta t = 0.008268$ a.u. and $k = 1$. We ran repeated simulations for increasing values of ℓ , each time recording the residual error at the final time T , $\text{residual}(T)$, defined by (56).

In Figure 7, for each of our four molecular systems, we plot $\text{residual}(T)$ as a function of total memory $k\ell\Delta t$. For the values of total memory shown, the residual errors are in the range $O(10^{-6})$ to $O(10^{-8})$; this corresponds to condition numbers of $M''(t)$ in the range of 10^8 to 10^{10} . The plotted residual errors are neither unacceptably large nor desirably small. Though $M''(t)$ may have full rank, for particular choices of system and simulation parameters, it is clearly ill-conditioned.

This is true despite the work we carried out in Section 4 to incorporate Hermitian symmetry, constant trace, and identically zero elements into (51)—these steps reduced the number of columns of $M''(t)$. This motivates future work to incorporate further properties of $P(t)$, such as its definition as a rank-1 matrix, into our propagation scheme for 1RDMs. If we can solve for still fewer elements of $P(t)$, then we can eliminate more columns of $M''(t)$, decreasing its condition number. We describe one such path, leading to a nonlinear model, in Section 6.

Results align with [17]. For the homogeneous electron gas perturbed by an electric field, [17] uses analytic methods to derive exchange-correlation functionals with memory for time-dependent current density functional theory (TDCDFT), a theory that is distinct from TDDFT. In [17], the memory kernels for the derived exchange-correlation functionals decay on a physical time scale of 10-20 a.u. This is within the same order of magnitude as all results reported here, despite the differences in methods and systems.

Further work is required to distill the relationship between memory-dependence and basis set. For each molecular system, as we increase the size of the basis set, we expect to compute more accurate electron dynamics. In the course of studying propagation method (52), we found a complex interrelationship between basis set, total memory, field frequency, and error. At some frequencies and choices of total memory, $Q_{\text{model}}(t)$ as computed by (52) agrees more closely with $Q_{\text{true}}(t)$ as the basis set size increases. For other choices of frequency and total memory, the opposite occurs. The differences may partially be explained by symmetries of the molecules we have chosen, which affect the Hamiltonian $H(t)$ and by extension our propagation scheme. For instance, due to the symmetry of the H_2 molecule, there is no permanent dipole moment in either the ground or excited state, and we therefore find that its corresponding dipole moment matrix M_{dip} has a zero diagonal. This has non-trivial implications for the numerics in (52) that rely on the pseudoinverse. All of this motivates future study, especially as we aim to quantify the memory-dependence of molecules on grids in real space (as in TDDFT), rather than in particular basis sets.

6 Conclusion

In this paper, we presented and derived a linear, closed time-delay system to propagate reduced 1-electron density matrices (1RDMs). To construct this system, we needed to understand the details of how to compute 1RDMs from full density matrices. Building on concepts and methods from quantum chemistry, we developed a mathematical formalism that enables full evaluation of the B tensor that relates full CI densities to 1RDMs. Using this formalism, we proved that the trace of the 1RDMs is constant and equals N , the total number of electrons. These results are general and do not depend on the basis set, number of electrons, or subset of Slater determinants that comprise the CI basis functions.

With B in hand, we derived (40), our first propagation scheme for 1RDMs. The main insight in this derivation was to add enough memory-based constraints—relating the full density at the present time to 1RDMs at past times—to change a linear system from underdetermined to overdetermined. Next, we accounted for properties of full density matrices: their Hermitian symmetry, constant trace, and zero elements that can be eliminated *a priori*. This resulted in the improved propagation scheme (52), which we implemented numerically and studied.

In our numerical tests, we focused on two 2-electron molecules (H_2 and HeH^+), each in two basis sets (STO-3G and 6-31G). For the resulting four molecular systems, we showed that the propagation scheme (52) produced highly accurate 1RDMs given a sufficient time delay. For

each molecular system, the accuracy of our propagation method improved as we increased total memory-dependence ($k\ell\Delta t$) measured not in time steps but in physical units of time. For fixed Δt , when we held the number of delay steps ℓ fixed but increased the stride k , we saw error approach machine precision. We also saw that the error of our propagation scheme is approximately invariant under refinement of Δt . This was a particularly important result, given that the true dynamics take place in continuous time.

The present study motivates three areas for future work. First, having developed mathematical methods to propagate 1RDMs that arise from CI wave functions, we are now well-positioned to address scientific questions. We aim to establish basis-independent physical time scales of memory-dependence. This will require disentangling the interdependence between memory-dependence, applied field parameters (including frequency, intensity, number of cycles), and the molecule as represented by its core Hamiltonian H_0 and dipole moment matrix M_{dip} . We also hope to understand the memory-dependence of 1RDMs for larger systems. As N increases and the number of basis functions increases, TDCASSCF with an all electron, full orbital active space will become intractable; in this case, other, more approximate methods such as TDCIS (time-dependent configuration interaction singles) can be used to compute ground truth 1RDMs [15, 10]. Compared to TDCASSCF, TDCIS has fewer excited states for electrons to enter. It will be of interest to study if and how approximations such as TDCIS impact the memory-dependence of 1RDMs.

Second, we can improve the propagation scheme (52). At present, the linear system (51) involves roughly half of the entries of $P(t)$ —the upper-triangular real and imaginary parts, including all but one element on the diagonal. Suppose we eliminate more columns from $M''(t)$ and thereby learn fewer entries of the rank-1 matrix $P(t) = \mathbf{a}(t)\mathbf{a}(t)^\dagger$. We can then formulate a quadratic programming problem to learn $\mathbf{a}(t)$ from our incompletely determined $P(t)$. Solving this at each time step, we could propagate $\mathbf{a}(t)$ forward in time, giving another route to propagate 1RDMs. The resulting method would be nonlinear, unlike the linear method we have derived in the present work. If enough columns could be eliminated from $M''(t)$, condition numbers would decrease, yielding greater accuracy.

Third, our work proves that there exists a time-dependent affine map that propagates 1RDMs forward in time; concretely, this affine map is the right-hand side of (52) not including $\mathbf{b}_\ell(t)$. Imagine if we could learn this time-dependent map without having to compute the Hamiltonian $H(t)$. Such a method would enable propagation of 1RDMs without the computational expense of running a static CI calculation to determine the core Hamiltonian H_0 . This would achieve the large-scale computational cost savings that reduced-order models seek, as mentioned in Section 1. It is an open question whether, for instance, machine learning methods could be used to learn the time-dependent affine map from data.

In Section 1.1, we mentioned the project of learning exchange-correlation potentials V_{xc} with memory-dependence on reduced 1-electron densities. In future work, we plan to use the methods developed in this paper (or improved versions thereof) to study memory-dependence of 1RDMs for a wide array of molecular systems in a broad set of field conditions, with the goal of achieving a comprehensive understanding of memory-dependence. This will enable a more robust and chemically insightful search of neural network architectures to accurately model and eventually learn V_{xc} in higher dimensions using, e.g., a three-dimensional version of the adjoint method derived in [2]. Learning memory-dependent V_{xc} functionals would bring TDDFT beyond the realm of the adiabatic approximation, fixing the egregious errors of commonly employed memory-independent potentials and enabling more accurate time-dependent electron dynamics simulations of molecules and materials.

Acknowledgements

Research was sponsored by the Office of Naval Research and was accomplished under Grant Number W911NF-23-1-0153. The views and conclusions contained in this document are those of the authors and should not be interpreted as representing the official policies, either expressed or implied, of the Army Research Office or the U.S. Government. The U.S. Government is authorized to reproduce and distribute reprints for Government purposes notwithstanding any copyright notation herein. We acknowledge support from the U.S. Department of Energy, Office of Science, Basic Energy Sciences under Award Number DE-SC0020203. H. Bassi acknowledges partial support from NSF DMS-1840265. This research used resources of the National Energy Research Scientific Computing Center (NERSC), a U.S. Department of Energy Office of Science User Facility located at Lawrence Berkeley National Laboratory, operated under Contract No. DE-AC02-05CH11231 using NERSC award BES-m2530 for 2021 and 2022. We also acknowledge computational time on the Pinnacles cluster at UC Merced, supported by NSF OAC-2019144.

References

- [1] Peter Benner, Tobias Breiten, Carsten Hartmann, and Burkhard Schmidt. Model reduction of controlled Fokker–Planck and Liouville–von Neumann equations. *Journal of Computational Dynamics*, 7(1):1–33, 2020. doi:10.3934/jcd.2020001.
- [2] Harish S. Bhat, Kevin Collins, Prachi Gupta, and Christine M. Isborn. Dynamic learning of correlation potentials for a time-dependent Kohn-Sham system. In Roya Firooz, Negar Mehr, Esen Yel, Rika Antonova, Jeannette Bohg, Mac Schwager, and Mykel Kochenderfer, editors, *Proceedings of The 4th Annual Learning for Dynamics and Control Conference*, volume 168, of *Proceedings of Machine Learning Research*, pages 546–558. PMLR, 23–24 Jun 2022. URL: <https://proceedings.mlr.press/v168/bhat22a.html>.
- [3] Harish S Bhat, Karnamohit Ranka, and Christine M Isborn. Machine learning a molecular Hamiltonian for predicting electron dynamics. *International Journal of Dynamics and Control*, 8:1089–1101, 2020. doi:10.1007/s40435-020-00699-8.
- [4] James Bradbury, Roy Frostig, Peter Hawkins, Matthew James Johnson, Chris Leary, Dougal Maclaurin, George Necula, Adam Paszke, Jake VanderPlas, Skye Wanderman-Milne, and Qiao Zhang. JAX: composable transformations of Python+NumPy programs, 2018. <http://github.com/google/jax>.
- [5] Steven L. Brunton, Marko Budišić, Eurika Kaiser, and J. Nathan Kutz. Modern Koopman Theory for Dynamical Systems. *SIAM Review*, 64(2):229–340, 2022. doi:10.1137/21M1401243.
- [6] Alexandre J. Chorin and Ole H. Hald. *Stochastic Tools in Mathematics and Science*. Springer New York, New York, NY, third edition, 2014. doi:10.1007/978-1-4614-6980-3.
- [7] Alexandre J Chorin, Ole H Hald, and Raz Kupferman. Optimal prediction and the Mori-Zwanzig representation of irreversible processes. *Proceedings of the National Academy of Sciences*, 97(7):2968–2973, 2000. doi:10.1073/pnas.97.7.2968.
- [8] Eric Darve, Jose Solomon, and Amirali Kia. Computing generalized Langevin equations and generalized Fokker–Planck equations. *Proceedings of the National Academy of Sciences*, 106(27):10884–10889, 2009. doi:10.1073/pnas.0902633106.

[9] Peter Elliott, Johanna I Fuks, Angel Rubio, and Neepa T Maitra. Universal dynamical steps in the exact time-dependent exchange-correlation potential. *Physical Review Letters*, 109(26):266404, 2012. doi:10.1103/PhysRevLett.109.266404.

[10] James B Foresman, Martin Head-Gordon, John A Pople, and Michael J Frisch. Toward a systematic molecular orbital theory for excited states. *The Journal of Physical Chemistry*, 96(1):135–149, 1992. doi:10.1021/j100180a030.

[11] Eberhard K. U. Gross and Neepa T. Maitra. Introduction to TDDFT. In Miguel A.L. Marques, Neepa T. Maitra, Fernando M.S. Nogueira, E.K.U. Gross, and Angel Rubio, editors, *Fundamentals of Time-Dependent Density Functional Theory*, pages 53–99. Springer Berlin Heidelberg, Berlin, Heidelberg, 2012. doi:10.1007/978-3-642-23518-4_4.

[12] Prachi Gupta, Harish S Bhat, Karnamohit Ranka, and Christine M Isborn. Statistical learning for predicting density-matrix-based electron dynamics. *Stat*, 11(1):e439, 2022. doi:10.1002/sta4.439.

[13] Bradley F. Habenicht, Noriyuki P. Tani, Makenzie R. Provorse, and Christine M. Isborn. Two-electron Rabi oscillations in real-time time-dependent density-functional theory. *The Journal of Chemical Physics*, 141(18):184112, 11 2014. doi:10.1063/1.4900514.

[14] W. J. Hehre, R. Ditchfield, and J. A. Pople. Self-consistent molecular orbital methods. XII. Further extensions of Gaussian-type basis sets for use in molecular orbital studies of organic molecules. *The Journal of Chemical Physics*, 56(5):2257–2261, 09 1972. doi:10.1063/1.1677527.

[15] So Hirata, Martin Head-Gordon, and Rodney J Bartlett. Configuration interaction singles, time-dependent Hartree–Fock, and time-dependent density functional theory for the electronic excited states of extended systems. *The Journal of Chemical Physics*, 111(24):10774–10786, 1999. doi:10.1063/1.480443.

[16] Mason Kamb, Eurika Kaiser, Steven L. Brunton, and J. Nathan Kutz. Time-delay observables for Koopman: Theory and applications. *SIAM Journal on Applied Dynamical Systems*, 19(2):886–917, 2020. doi:10.1137/18M1216572.

[17] Yair Kurzweil and Roi Baer. Time-dependent exchange-correlation current density functionals with memory. *The Journal of Chemical Physics*, 121(18):8731–8741, 2004. doi:10.1063/1.1802793.

[18] J. Nathan Kutz, Steven L. Brunton, Bingni W. Brunton, and Joshua L. Proctor. *Dynamic Mode Decomposition: Data-Driven Modeling of Complex Systems*. SIAM, 2016. doi:10.1137/1.978161974508.

[19] Lionel Lacombe and Neepa T Maitra. Developing new and understanding old approximations in TDDFT. *Faraday Discussions*, 224:382–401, 2020. doi:10.1039/D0FD00049C.

[20] Yen Ting Lin, Yifeng Tian, Daniel Livescu, and Marian Anghel. Data-driven learning for the Mori-Zwanzig formalism: A generalization of the Koopman learning framework. *SIAM Journal on Applied Dynamical Systems*, 20(4):2558–2601, 2021. doi:10.1137/21M1401759.

[21] Volkhard May and Oliver Kühn. *Charge and Energy Transfer Dynamics in Molecular Systems*. Wiley-VCH, Weinheim, Germany, fourth edition, 2023. doi:10.1002/9783527633791.

[22] R. McWeeny. *Methods of Molecular Quantum Mechanics*. Chemistry, Physical and Theoretical. Academic Press, second edition, 1989.

[23] Hazime Mori. Transport, Collective Motion, and Brownian Motion. *Progress of Theoretical Physics*, 33(3):423–455, 03 1965. doi:10.1143/PTP.33.423.

[24] Y Ohtsuki and Y Fujimura. Bath-induced vibronic coherence transfer effects on femtosecond time-resolved resonant light scattering spectra from molecules. *The Journal of Chemical Physics*, 91(7):3903–3915, 1989. doi:10.1063/1.456822.

[25] Ryosuke Okuta, Yuya Unno, Daisuke Nishino, Shohei Hido, and Crissman Loomis. Cupy: A numpy-compatible library for nvidia gpu calculations. In *Proceedings of Workshop on Machine Learning Systems (LearningSys) in The Thirty-first Annual Conference on Neural Information Processing Systems*, 2017. URL: http://learningsys.org/nips17/assets/papers/paper_16.pdf.

[26] Jeppe Olsen, Björn O Roos, Poul Jørgensen, and Hans Jørgen Aa. Jensen. Determinant based configuration interaction algorithms for complete and restricted configuration interaction spaces. *The Journal of Chemical Physics*, 89(4):2185–2192, 1988. doi:10.1063/1.455063.

[27] Shaowu Pan and Karthik Duraisamy. On the structure of time-delay embedding in linear models of non-linear dynamical systems. *Chaos: An Interdisciplinary Journal of Nonlinear Science*, 30(7), 2020. doi:10.1063/5.0010886.

[28] Wei-Tao Peng, B Scott Fales, and Benjamin G Levine. Simulating electron dynamics of complex molecules with time-dependent complete active space configuration interaction. *Journal of Chemical Theory and Computation*, 14(8):4129–4138, 2018. doi:10.1021/acs.jctc.8b00381.

[29] Makenzie R. Provorose, Bradley F. Habenicht, and Christine M. Isborn. Peak-shifting in real-time time-dependent density functional theory. *Journal of Chemical Theory and Computation*, 11(10):4791–4802, 2015. PMID: 26574268. doi:10.1021/acs.jctc.5b00559.

[30] Karnamohit Ranka and Christine M. Isborn. Size-dependent errors in real-time electron density propagation. *The Journal of Chemical Physics*, 158(17):174102, 05 2023. doi:10.1063/5.0142515.

[31] Dmitrij Rappoport and Jürg Hutter. Excited-State Properties and Dynamics. In Miguel A.L. Marques, Neepa T. Maitra, Fernando M.S. Nogueira, E.K.U. Gross, and Angel Rubio, editors, *Fundamentals of Time-Dependent Density Functional Theory*, pages 317–336. Springer Berlin Heidelberg, Berlin, Heidelberg, 2012. doi:10.1007/978-3-642-23518-4\16.

[32] Björn O. Roos, Peter R. Taylor, and Per E.M. Sigbahn. A complete active space scf method (casscf) using a density matrix formulated super-CI approach. *Chemical Physics*, 48(2):157–173, 1980. doi:10.1016/0301-0104(80)80045-0.

[33] Erich Runge and Eberhard K. U. Gross. Density-functional theory for time-dependent systems. *Physical Review Letters*, 52(12):997, 1984. doi:10.1103/PhysRevLett.52.997.

[34] Takeshi Sato and Kenichi L. Ishikawa. Time-dependent complete-active-space self-consistent-field method for multielectron dynamics in intense laser fields. *Phys. Rev. A*, 88:023402, Aug 2013. doi:10.1103/PhysRevA.88.023402.

- [35] Boris Schäfer-Bung, Carsten Hartmann, Burkhard Schmidt, and Christof Schütte. Dimension reduction by balanced truncation: Application to light-induced control of open quantum systems. *The Journal of Chemical Physics*, 135(1):014112, 07 2011. doi:10.1063/1.3605243.
- [36] Yasumitsu Suzuki, Ryo Nagai, and Jun Haruyama. Machine learning exchange-correlation potential in time-dependent density-functional theory. *Phys. Rev. A*, 101:050501, May 2020. doi:10.1103/PhysRevA.101.050501.
- [37] Attila Szabo and Neil S. Ostlund. *Modern Quantum Chemistry: Introduction to Advanced Electronic Structure Theory*. Dover Publications, 2012. “Unabridged, unaltered republication of the ‘First Edition, Revised, originally published by McGraw-Hill, New York in 1989’.”
- [38] Floris Takens. Detecting strange attractors in turbulence. In *Dynamical Systems and Turbulence, Warwick 1980*, pages 366–381. Springer, 1981. doi:10.1007/BFb0091924.
- [39] Carsten Ullrich. *Time-Dependent Density-Functional Theory: Concepts and Applications*. Oxford Graduate Texts. Oxford University Press, Oxford, 2012. doi:10.1093/acprof:oso/9780199563029.001.0001.
- [40] Fuzhen Zhang. *The Schur Complement and Its Applications*. Springer US, New York, NY, First edition, 2005. doi:10.1007/b105056.
- [41] Robert Zwanzig. Memory effects in irreversible thermodynamics. *Phys. Rev.*, 124:983–992, Nov 1961. doi:10.1103/PhysRev.124.983.
- [42] Robert Zwanzig. On the identity of three generalized master equations. *Physica*, 30(6):1109–1123, 1964. doi:10.1016/0031-8914(64)90102-8.